

ANNUAL TECHNICAL REPORT 1987
on
Earthquake Monitoring of Eastern Washington

October 1987

Geophysics Program
University of Washington
Seattle, Washington

This report was prepared as an account of work sponsored by the United States Government. Neither the United States nor the Department of Energy, nor any of their employees, nor any of their contractors, subcontractors, or their employees, makes any warranty, express or implied, or assumes any legal liability or responsibility for the accuracy, completeness or usefulness of any information, apparatus, product or process disclosed, or represents that its use would not infringe privately-owned rights.

By acceptance of this article, the publisher and/or recipient acknowledges the U.S. Government's right to retain a non-exclusive, royalty-free license in and to any copyright covering this paper.

PREPARED FOR THE U.S. DEPARTMENT OF ENERGY
UNDER CONTRACT NO. EY-76-S-06-2225
TASK AGREEMENT NO. 39

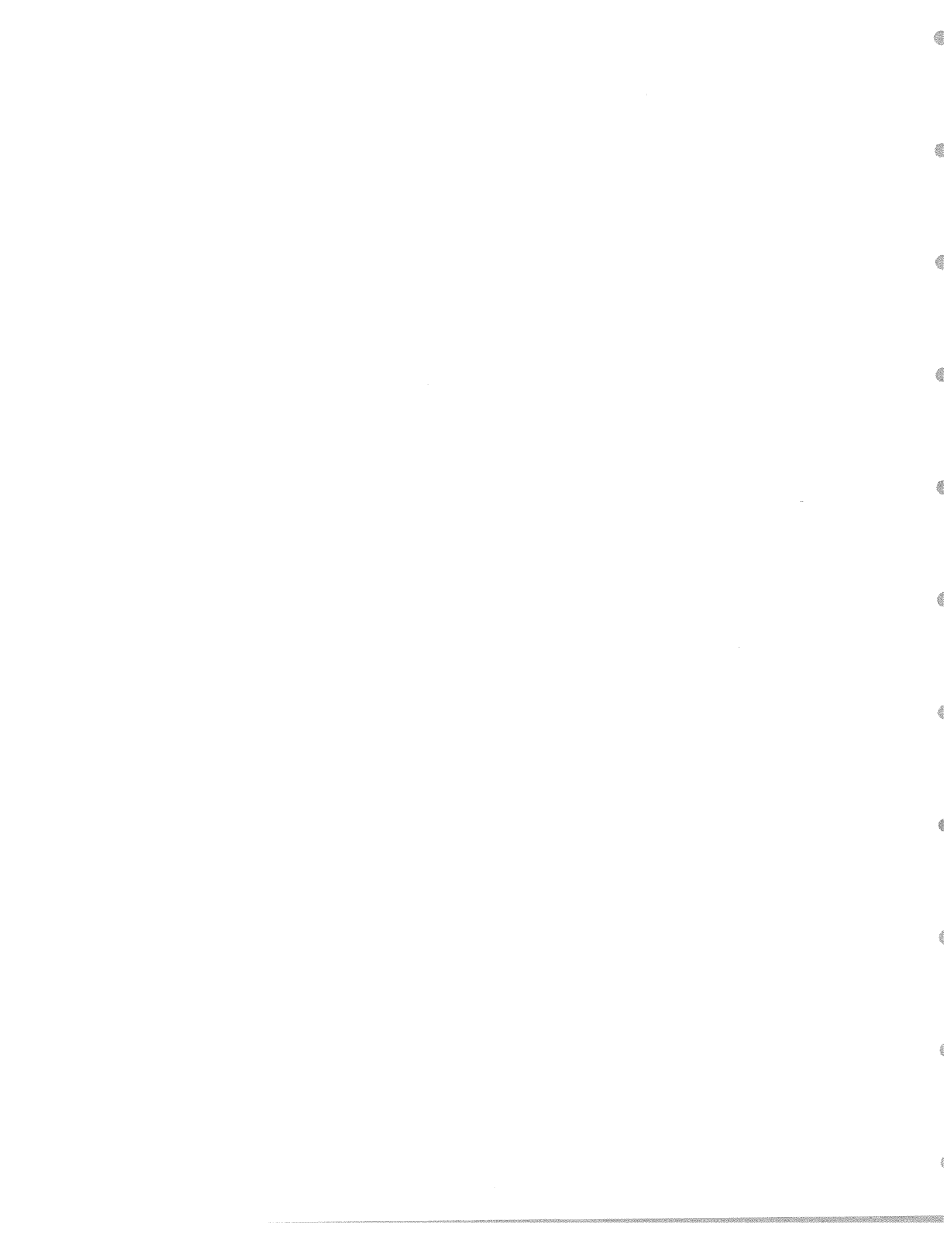


TABLE OF CONTENTS

I.....	Introduction and Operations	3
II	Seismicity July 1, 1986 - June 30, 1987	18
III.....	Focal Mechanism Summary.....	28
IV.....	Earthquake Sequence Analysis	44
V.....	Hypocenter Determination Comparison	54
VI.....	Coda-Q Study	61
Appendix I	Eastern Washington Catalog 1986-1987	76

Edited by:

Stephen Malone

Contributions by:

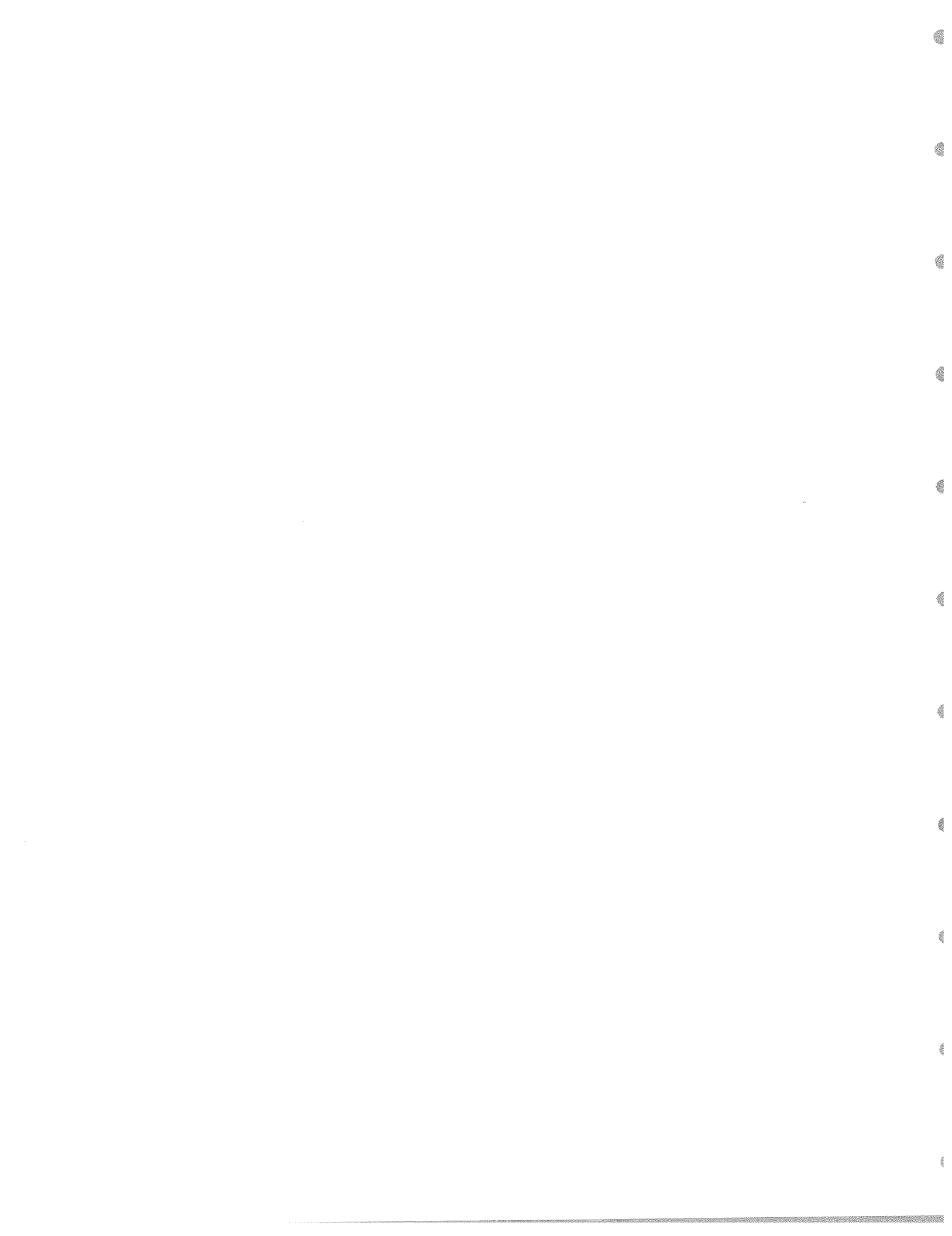
Peggy Johnson-Browne

Dai McClurg

Tony Qamar

Jim Ramey

Keri Thompson



I - INTRODUCTION AND OPERATIONS

Introduction

This report covers the operations and research performed for D.O.E. by the University of Washington Geophysics Program on the seismicity and structure of eastern Washington and northeastern Oregon for the year, July 1, 1986 to June 30, 1987. This contract helps support parts of the Washington state regional seismograph network. There are presently 117 stations in Washington and northeastern Oregon whose data are telemetered to the University for recording, analysis and interpretation. The Department of Energy supports the stations on the east flank of the Cascades and throughout eastern Washington and northeastern Oregon. Other parts of the network are supported by the U.S. Geological Survey. Figure I-1 shows all of the stations of the state-wide network and Table I-1 lists the 43 stations supported by this DOE contract.

Section I of this report covers the operation of the network including station maintenance and calibration, data processing and operational problems for the past year in eastern Washington. A detailed description of the current network including telemetry routing through the BPA microwave system is included. This section also details a new VCO system developed here to improve the center-frequency stability and reliability of our field stations. The seismicity of the past year and a description of the catalog is covered in section II. Section III is a description of preliminary work on producing a comprehensive catalog of focal mechanisms for events in eastern Washington. Continued work on the study of earthquake clustering is included in section IV. Section V is a comparison of three different earthquake hypocenter determination programs which has been done to benchmark routines used locally with those used at other institutions. We include in section VI part of a state-wide coda-Q study applicable to a comparison of eastern Washington with the rest of the state. The appendix includes the catalog of earthquakes located in eastern Washington during the year.

Network Operations

The 43 stations of the eastern Washington network operated with no major problems for the past year. Table I-1 lists the stations supported under this contract and figure I-1 shows all the stations of the state-wide network. Stations east of the 121°W in the Cascades are supported by this contract. As of late summer, 1987 we are beginning an expansion farther into Oregon under U.S. Geological Survey sponsorship. Five new stations will be added to the east-central Oregon Cascade area this fall. Next summer an additional thirteen stations will complete this expansion and will include stations as far south as Crater Lake and also several stations in the Oregon Coast range.

All connections to BPA channels for transmitting our seismic data via microwave to the UW recording labs were completed during the past year. These connections required working with BPA engineering, providing them with sketches of our physical layout at each site, listings of radio frequencies used, and coordinating our installations with their field engineers responsible for each site. There were also hardware items designed and constructed or purchased to meet BPA's safety and construction requirements. Several BPA radio towers varied in structure and required special hardware and installation techniques. All BPA personnel have been very helpful during this operation.

The location of the BPA sites made it necessary for us to rearrange the radio telemetry paths of our network. A detailed layout of our current eastern Washington seismic stations and their radio paths to all BPA microwave sites are summarized in Table I-2 and figures I-2A to I-2H. This includes both VCO and radio transmitter frequencies for each station. A schematic of the BPA lines from field sites to Seattle is shown in figure I-3. New radio paths were chosen to minimize station relocation and to maintain the integrity of the existing network. All major radio receiver sites which had previously been connected to telephone lines were transmitted instead to BPA receiver sites via UHF radios. All phone drops were discontinued and the stations involved were converted to VHF radio telemetry by transmission to an existing radio repeater site or by transmission to a BPA

site directly. Several seismograph sites had to be moved to make possible the radio links to BPA. Five stations required significant relocation (EST to TWW, WGW to WGE, MFW to LNO, PEN to CHO, ETT to ETW) and ten stations were converted from phone drop terminations to VHF radio telemetry. One station (FOX) was removed and two new stations (BVW, DPW) were added. All these changes were made so that there would be no radio or VCO frequency conflicts.

All changes were made by mid-November, 1986 with minimal interruption to the recording of data during the changeover. Our last phone billing period was for October, 1986. The BPA facilities have proven to be of very consistent high quality, and any problems have been minor and easily corrected.

Fourteen stations were converted from battery-only power to solar power with battery back-up as they were visited or moved. There are now a total of twenty three solar powered sites. Those seismograph stations at BPA sites are operating on commercial line power. Summaries of station operation histories as determined by the repair logs and by reviewing records of teleseisms has been published in each quarterly technical report. We no longer use the real-time P-picker for reliable determination of station down-time.

Improved Field VCO

In October, 1986 a functional prototype of our proposed VCO design was built. This wire-wrap prototype was placed in the crater at Mount St. Helens as part of a sound detection system to detect audible events in the crater. This VCO unit is still in operation today. After it had run successfully for several months at Mount St. Helens we decided to design a printed circuit board version for use at our regular seismograph sites.

Until recently we have been able to purchase new VCO units and spare parts for our existing units at reasonable cost. Few commercial VCO units are available now and they are very expensive. Spare parts for some of our units are currently unavailable.

There were several criteria which we wanted to have incorporated into the design of a

new VCO. Most important was the temperature stability of the VCO center-frequency. Also important were low power consumption, switch selectable center frequency, compatibility with existing equipment, deviation linearity, and the availability of easily acquired parts. We wanted to achieve all these elements with minimal circuit complexity. All previous VCO's have used a feedback bias current with a nearly linear temperature sensing device for temperature stability. This bias-feedback circuit usually takes quite a while to stabilize prior to putting a VCO in the field. We decided to design a means of counting the VCO frequency and use this count to control the frequency controlling bias on a 4046 Phase Locked Loop. After investigation of several CMOS micro-controller Units from Intel and discussions with several people who had worked with them, we decided to use the 80C31 MCU which has built-in counters, has very low power consumption, can be programed to provide additional functions, and is easily acquired.

Peter Mullen, a graduate student in the Geophysics Program, who has worked with the MCU devices in Sample-and-Hold circuits, wrote all the computer assembly routines we now use. The logic flow for this system is shown in figure I-4. His design uses the MCU to control a VDC (variable duty cycle) pulse train to an RC circuit which is transferred through a MOSFET device by a clock control pulse to provide a bias at the frequency control pin of a 4046 PLL. The MCU controls the VDC by counting the output frequency of the PLL which is oscillating at 10 times the final output frequency. After determining that this configuration would work we added a switch selectable center-frequency feature.

In our inventory we have many incomplete Develco 6202 AMP-VCO units. Many 6202 units are still in use at sites in eastern Washington. Last winter our new VCO circuit board was designed to fit in the 6202 chassis (figure I-5), and six VCO boards were initially built. There is one new amp-VCO running at the TWW site, and we plan to operate other units at several other easily accessible sites to test the VCO's dependability. The VCO cards cost approximately \$180 each to construct. The cost may be reduced as more cards are built.

We plan to alter the assembly program controlling the 80C31 MCU in the near future to provide a daily calibration pulse, and to provide a digital data stream output at any selected baud rate. Both of these features should be easily incorporated into the software.

Specifications for the new VCO (As installed in 6202 motherboard):

- A Voltage Regulator-Converter:2 included, 1 on VCO card for isolation. PreAmp,AMP,Filter 10-15vdc input ± 9 vdc output VCO 5.5-15vdc input ± 5 vdc output
- B PreAmp-- X1000 fixed gain, 10K input impedance,differential amp.
- C Filter--2-pole Butterworth bandpass filter response with -3dB bandwidth of 0.1 to 30Hz (12dB/octave rolloff below 0.1Hz and above 30Hz).
- D Amp--gain adjustment attenuation in 6dB steps from 120dB maximum gain.
- E VCO-- switch selectable for 8 center-frequencies,input impedance of 100K ohms,deviation adjustable for ± 125 Hz, operating temperature stability of oscillator frequency 0.0005%/ $^{\circ}$ C, operating temperature range -40 to +75 $^{\circ}$ C, digitally generated sine wave at 1/10 oscillator frequency, lowpass output filter to transformer, output level adjustable to C+-4vpp.
- F Power--16ma total @ 13.5vdc

Seismograph Calibration

In Table I-1, seismograph stations in eastern Washington which have a known ground response as a function of frequency are highlighted by an asterisk (*) next to their names. The number of such stations will increase as we replace seismometers and VCO/amplifiers in the field with calibrated components. The frequency response of the seismograph system is regarded as the product of several simple analytic functions of frequency as described in Healy and O'Neill (1977)*. In the laboratory, we determine the free parameters of the analytic functions which best describe the component being tested. Such free parameters include the free period and damping of the seismometer, cutoff frequencies and rolloff characteristics of filters in amplifier/VCOs and discriminators, etc. Our procedures can be summarized as follows:

1. Amplifier/VCOs are all adjusted in the laboratory so that at a gain of 60 dB the amplifier stage yields ± 1.0 volt out for a ± 1 mv, 1 Hz sine wave at the input. In the field, the amplifier is set to a gain which is generally different than 60dB depending on

*Healy, J.H., M.E. O'Neill, 1977, Calibration of Seismograph Systems: USGS stations in the central California network, *US Geological Survey Open File Report 77-736*.

the level of local ground noise. With the seismometer connected to the amplifier/VCO an appropriate gain yields a response to ground noise of about 100 mv peak-to-peak at the output of the amplifier. The VCO section of the amplifier-VCO is adjusted to a sensitivity of 41.67Hz/volt.

2. Discriminators are adjusted to a sensitivity of 1 volt/41.67 Hz. The frequency response of different types of discriminators and amplifier/VCOs at very high and very low frequency is determined in the lab using a sine wave function generator.
3. The response of the seismometer to ground velocity at frequency f is assumed to be $G_e[\omega^2/D(\omega)]$ volts-sec/meter, where $D(\omega) = [(\omega^2-\omega_o^2)^2 + 4\beta^2\omega_o^2\omega^2]^{1/2}$, $\omega=2\pi f$, $\omega_o=2\pi f_o$, f_o is the natural frequency of the seismometer in Hz, β is the damping coefficient (fraction of critical) and G_e is the effective electrodynamic constant of the signal coil at the amplifier input. In the field, a damping resistor (r_d) is placed across the output of the seismometer's signal coil resistance (r_s). The input resistance (r_a) of the field amplifier is also in parallel with r_d . Hence, $G_e = G[1+r_s(1/r_d+1/r_a)]^{-1}$, where G is the intrinsic electrodynamic coil constant. In the laboratory we determine G by a least squares procedure using observed values of damping β with various resistors, r_e , placed across the output of an isolated seismometer. Theoretically, $G=[4\pi f_o M(r_e+r_s)(\beta-\beta_o)]^{1/2}$, where M is the mass of the seismometer and β_o is the intrinsic damping of the seismometer with no external resistance connected. Seismometer damping is determined in the laboratory from analysis of waveforms recorded by a Nicolet digital storage oscilloscope. The value of r_d used in the field is normally chosen so that the seismometer damping $\beta=0.8$.
4. The sensitivity of the digitizer linked to the DEC PDP 11/34 computer which records the seismic signal is 411.2 counts/volt. Its frequency response is flat in the bandwidth of interest (0-50 Hz).

Figure I-6 shows typical frequency responses of calibrated seismograph components.

Table I-1 DOE Supported or Related Stations 1986-87

Station designator	Latitude(N) (dg mn sec)	Longitude(W) (dg mn sec)	Elevation (km)	Station name
BRV	46 29 07.2	119 59 29.4	0.925	Black Rock Valley
BVW	46 48 37.8	119 52 54.1	0.707	Beverly
CBW	47 48 25.5	120 01 57.6	1.160	Chelan Butte
CHO	45 35 27.0	118 34 45.0	1.076	Cabbage Hill, Oregon
CRF	46 49 30.6	119 23 18.0	0.260	Corfu
DPW*	47 52 14.3	118 12 10.2	0.892	Davenport
DY2	47 59 06.9	119 46 13.0	0.884	Dyer Hill 2
ELL	46 54 35.0	120 34 06.0	0.805	Ellensburg
EPH	47 21 12.8	119 35 46.2	0.628	Ephrata
ETP	46 27 53.4	119 03 32.4	0.250	Eltopia
ETW*	47 36 16.2	120 19 51.6	1.475	Entiat
FOX*	48 19 50.0	119 42 29.0	0.896	Fox Mountain
GBL*	46 35 51.6	119 27 35.4	0.330	Gable Mountain
GL2	45 57 35.0	120 49 22.5	1.000	New Goldendale
HH2	46 10 18.0	119 23 01.0	0.490	Horse Heaven Hills
LNO	45 52 15.8	118 17 06.0	0.768	Linton Mt., Oregon
MDW*	46 36 48.0	119 45 39.0	0.330	Midway
MOX	46 34 38.0	120 17 35.0	0.540	Moxie City
NAC	46 44 03.8	120 49 33.2	0.738	Naches
NEL	48 04 41.8	120 20 17.7	1.490	Nelson Butte
NEW	48 15 50.0	117 07 13.0	1.000	Newport Observatory (USGS)
ODS	47 18 24.0	118 44 42.0	0.523	Odessa
OTH	46 44 20.4	119 12 59.4	0.260	Othello
PAT	45 52 50.1	119 45 40.1	0.300	Paterson
PRO	46 12 45.6	119 41 09.0	0.552	Prosser
RPK	45 45 42.0	120 13 50.0	0.330	Roosevelt Peak
RSW	46 23 28.2	119 35 19.2	1.037	Rattlesnake Mt. (East)
SAW	47 42 06.0	119 24 03.6	0.690	St. Andrews
SYR	46 51 46.8	119 37 04.2	0.267	Smyrna
TBM	47 10 10.1	120 35 54.0	1.064	Table Mt.
TWW	47 08 17.2	120 52 04.5	1.046	Teanaway
VGB	45 30 56.4	120 46 39.0	0.729	Gordon Butte, Oregon
VIP	44 30 29.4	120 37 07.8	1.731	Ingram Pt., Oregon
VTG	46 57 28.8	119 59 14.4	0.208	Vantage
VTH*	45 10 52.2	120 33 40.8	0.773	The Trough, Oregon
WA2	46 45 24.2	119 33 45.5	0.230	Wahluke Slope
WAT	47 41 55.0	119 57 15.0	0.900	Waterville
WBW	48 01 04.2	119 08 13.8	0.825	Wilson Butte
WEN	47 31 46.2	120 11 39.0	1.061	Wenatchee
WGE	46 03 09.0	118 48 08.0	0.262	Wallula Gap East
WIW	46 25 48.8	119 17 13.4	0.130	Wooded Island
WNS	46 42 37.0	120 34 30.0	1.000	Wenas
WRD	46 58 11.4	119 08 36.0	0.378	Warden
YAK	46 31 15.8	120 31 45.2	0.619	Yakima

* Calibrated station

Hanford Stations

Table I-2

STA	latd	latm	latS	lngd	lngm	lngs	install	Station name	Rx For:	Tx	to	Dist. Km
UW	47	39	18	122	18	30		Univ.of Washington	✓			
BPA												
QAB	47	39	16	122	23	42	6/86	Queen Anne BPA	✓ BPA lines in Seattle			
WVB	47	35	17.8	120	8	31.7	7/11/86	Waterville,BPA	✓ CBW,ETW,WEN,WAT,WBW,DY2,SAW	line		
DVB	47	52	14.3	118	12	10.2	11/7/86	Davenport,BPA	✓	line		
ECC	47	10	54.5	119	19	12.4	11/18/86	ECC Moses Lake,BPA	✓ EPH	line		
BVB	46	48	37.5	119	52	54.1	7/24/86	Beverly,BPA	✓ VTG,RCH,BVW(line)	line		
ASB	46	28	45	119	20	4.3	6/13/86	Ashe,BPA	✓ GBL	line		
KWB	46	6	15.4	119	7	50.8	7/28/86	Kennewick,BPA	✓ WG2,RSW	line		
SSB	46	29	9.1	119	59	29	11/5/86	Sunnyside,BPA	✓ YAK,BRV(line)	line		
TWB	47	8	17.2	120	52	4.5	10/24/86	Teanaway,BPA	✓ TBM,TWW(line)	line		
WCB	45	30	57.4	120	46	38.7	6/3/86	Wasco,BPA	✓ GL2,VBE,RPK,JBO,VGB(line)	line		
<i>Stas.</i>												
BVW	46	48	37.5	119	52	54.1	9/30/86	Beverly,WA	✓	line	BVB	
BRV	46	29	7.2	119	59	29.4	12/83	Black Rock Valley	✓	line	SSB	
CBW	47	48	25.5	120	1	57.6	6/12/75	Chelan Butte	NEL,CBW(line)	416.806	WVB	26
CHO	45	35	27	118	34	45	8/26/86	Cabbage Hill OR	*	171.218	WG2	65
CRF	46	49	30.6	119	23	18	6/3/74	Corfu	*	219.35	SYR	18
DPW	47	52	14.3	118	12	10.2	11/7/86	Davenport WA	✓	line	DVB	
DY2	47	59	6.91	119	46	13.03	6/19/85	Dyer Hill		163.396	WVB	52
ELL	46	54	35	120	34	6	6/79	Ellensburg		171.218	TBM	29
EPH	47	21	12.8	119	35	46.2	3/8/83	Ephrata	*	171.406	ECC	28
ETP	46	27	53.4	119	3	32.4	6/1/75	Eltopia	*	219.65	RSW	42
ETW	47	36	16.2	120	19	51.6	10/1/86	Entiat		162.809	WVB	14
GBL	46	35	51.6	119	27	35.4	6/4/74	Gable	✓ MDW,WA2,OTH,WTW,HHW,GBL(line)	419.996	ASB	16
GL2	45	57	50	120	49	15	9/84	New Goldendale		166.418	WCB	46
HH2	46	10	18	119	23	1	3/27/87	Horse Heaven 2nd	*	219.25	GBL	48
JBO	45	27	41.7	119	50	13.28	9/30/82	Jordan Butte, Ore	*	171.406	WCB	75
LNO	45	52	15.8	118	17	6	8/27/86	Linton Mtn OR	*	165.806	WG2	48
MDW	46	36	48	119	45	39	6/2/74	Midway	*	219.5	GBL	23
MOX	46	34	38	120	17	35	10/5/84	Moxie City	*	219.35	YAK	19
NAC	46	44	3.8	120	49	33.2	6/79	Naches		167.193	YAK	33
NEL	48	4	41.8	120	20	17.7	5/30/85	Nelson Butte	*	167.809	CBW	38
ODS	47	18	24	118	44	42	6/13/75	Odessa	*	219.6	EPH	65
OTH	46	44	20.4	119	12	59.4	6/75	Othello		173.194	GBL	25
PAT	45	52	50.1	119	45	40.1	4/21/81	Paterson	*	163.396	RSW	58
PRO	46	12	45.6	119	41	9	5/31/75	Prosser	*	164.846	RSW	21
RCH	46	54	48	119	37	32.2	7/23/86	Royal City High School	*	219.4	BVB	10
RPK	45	45	42	120	13	50	8/84	Roosevelt Peak	*	159.565	WCB	49
RSW	46	23	28.2	119	35	19.2	6/3/75	RattleSnake	PRO,PAT,ETP,RSW(line)	416.809	KWB	48
SAW	47	42	6	119	24	3.6	6/8/75	St. Andrews		164.846	WVB	57
SYR	46	51	46.8	119	37	4.2	6/3/75	Smyrna	*	173.61	RCH	6
TBM	47	10	10	120	35	58	7/23/79	Table Mt.	*	171.43	TWB	18
TWW	47	8	17.2	120	52	4.5	10/24/86	Teanaway	✓	line	TWB	
VBE	45	3	37.2	121	35	12.6	10/25/79	Beaver Butte	*	169.575	WCB	84
VGB	45	30	56.4	120	46	39	4/11/80	Gordon Butte	✓	line	WCB	
VTG	46	57	28.8	119	59	14.4	6/12/75	Vantage	*	163.796	BVB	16
WA2	46	45	24.2	119	33	45.5	5/9/78	Wahluke Slope	*	167.809	GBL	19
WAT	47	41	55	119	57	15	11/76	Waterville		173.49	WVB	19
WBW	48	1	4.2	119	8	13.8	6/9/75	Wilson Butte	*	166.421	WVB	89
WEN	47	31	46.2	120	11	39	6/13/75	Wenatchee		160.515	WVB	8
WGT	46	1	43	118	51	24	4/23/87	Walla Walla Gap 2nd	*	171.406	KWB	20
WTW	46	25	48.8	119	17	13.4	6/4/74	Wooded Island		219.3	GBL	23
WNS	46	42	37	120	34	30	7/15/84	Wenas	*	219.55	YAK	21
WRD	46	58	11.4	119	8	36	6/6/75	Werden		219.4	EPH	55
YAK	46	31	15.8	120	31	45.2	6/4/79	Yakima	NAC,MOX,WNS,YAK(line)	219.3	SSB	43
								✓ LinePower				
								* Solar Power				
								All others aircells				

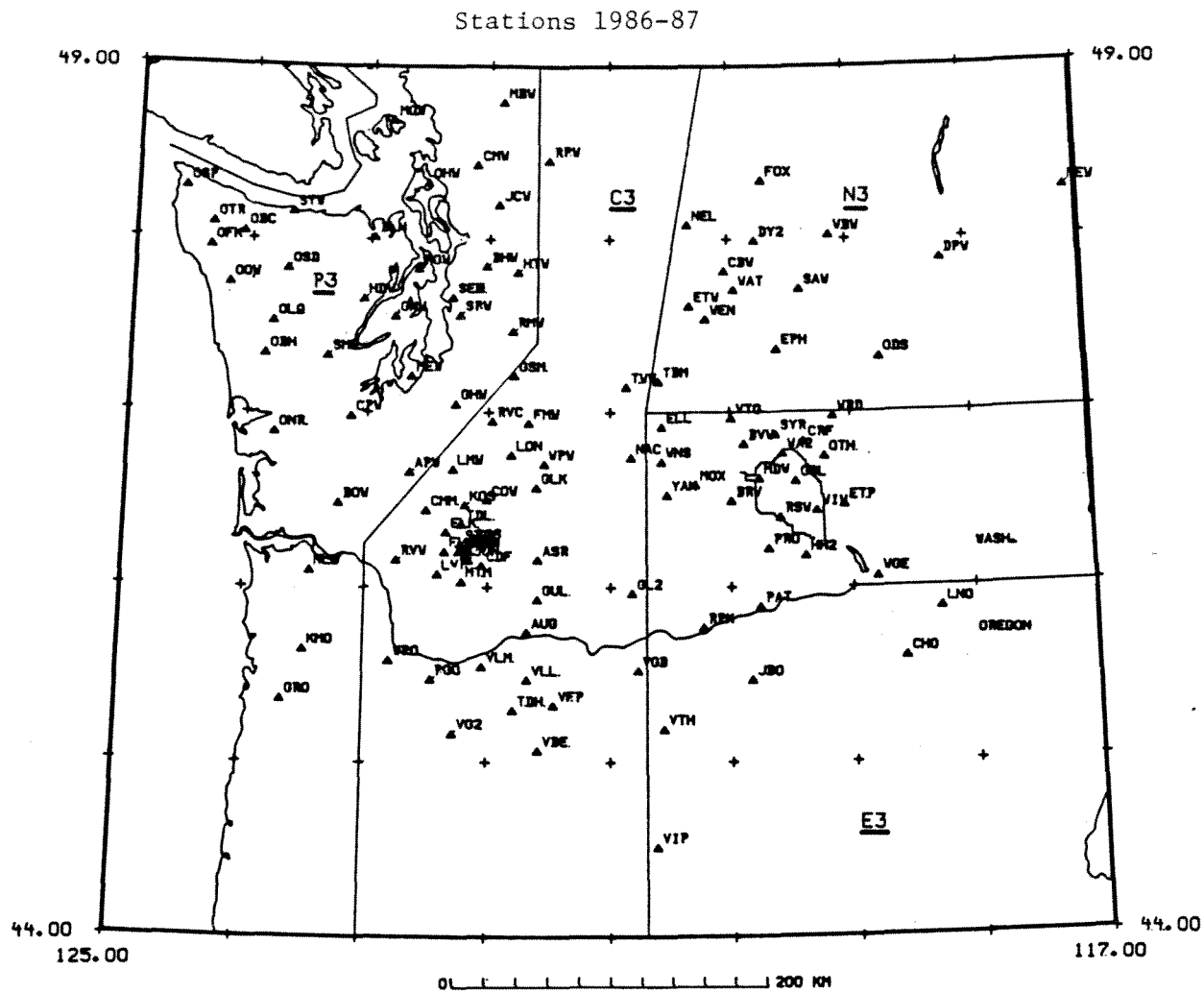


Figure I-1. Seismograph stations operating in the period July 1, 1986 to June 30, 1987. The Department of Energy supports stations east of 121°W. Thin, straight lines outline regions in which different velocity models are used (P3, C3, N3, E3) to locate earthquakes. The outline of the Hanford reservation is also shown in southeast Washington.

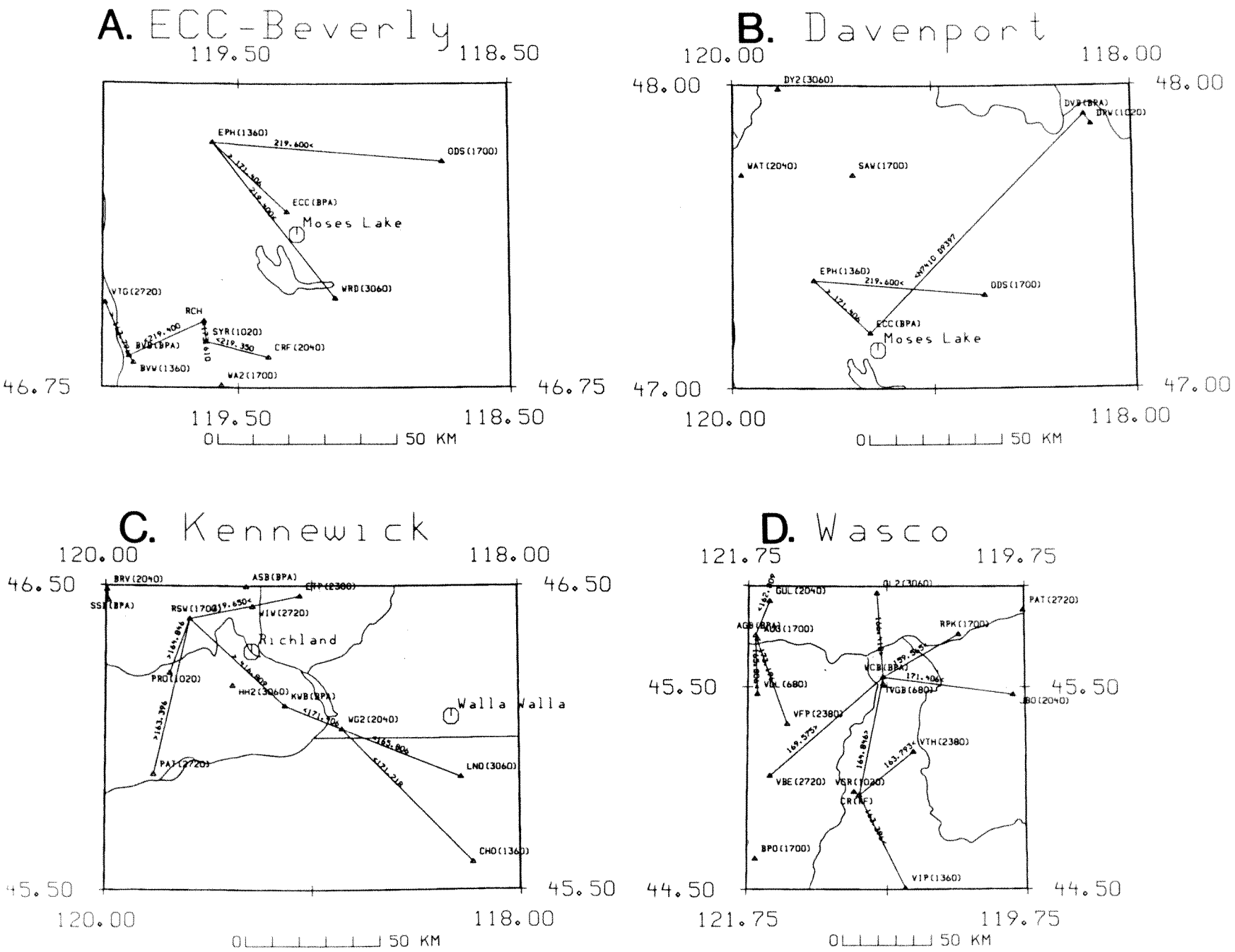


Figure I-2 A-D. Detailed maps of the telemetry routes for each BPA microwave channel. VCO center frequency (in Hz) is shown in parentheses and VHF radio frequency (in MHz) is shown along telemetry paths.

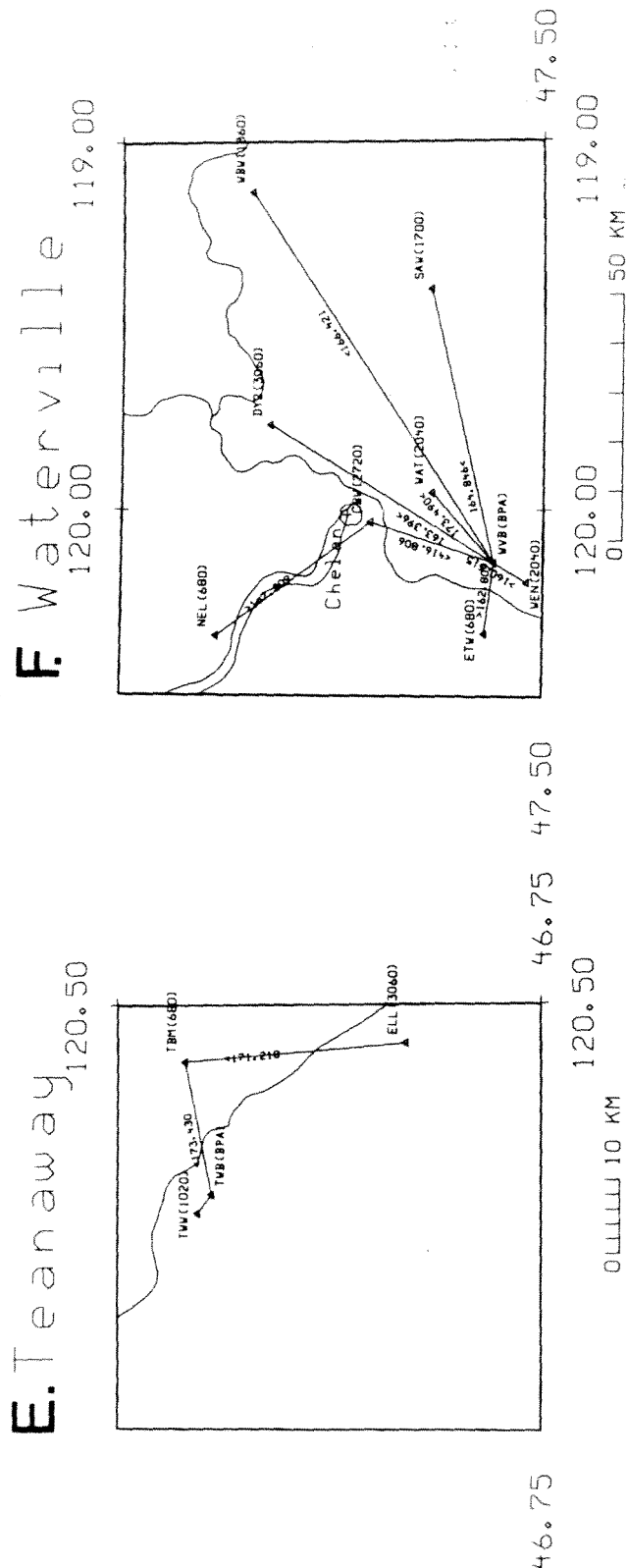


Figure I-2 E-H. Detailed maps of the telemetry routes for each BPA microwave channel. VCO center frequency (in Hz) is shown in parentheses and VHF radio frequency (in MHz) is shown along telemetry paths.

Hanford Network - BPA channels

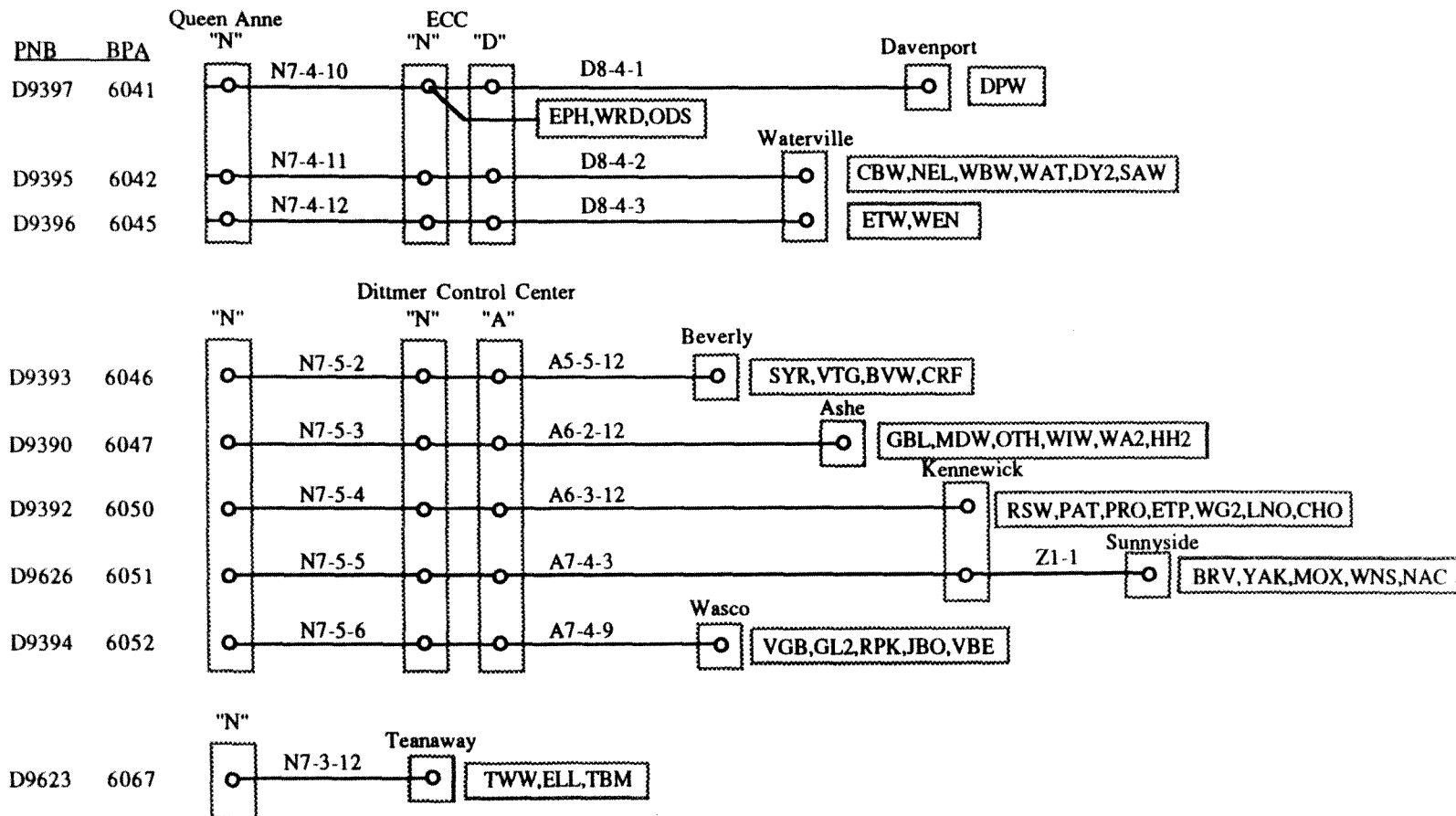


Figure I-3 Summary of BPA microwave channels for eastern Washington. PNB column is for the phone line between Queen Anne BPA receiver and the University; BPA column is the BPA designator; the other numbers along each line are for the individual BPA network system channel numbers

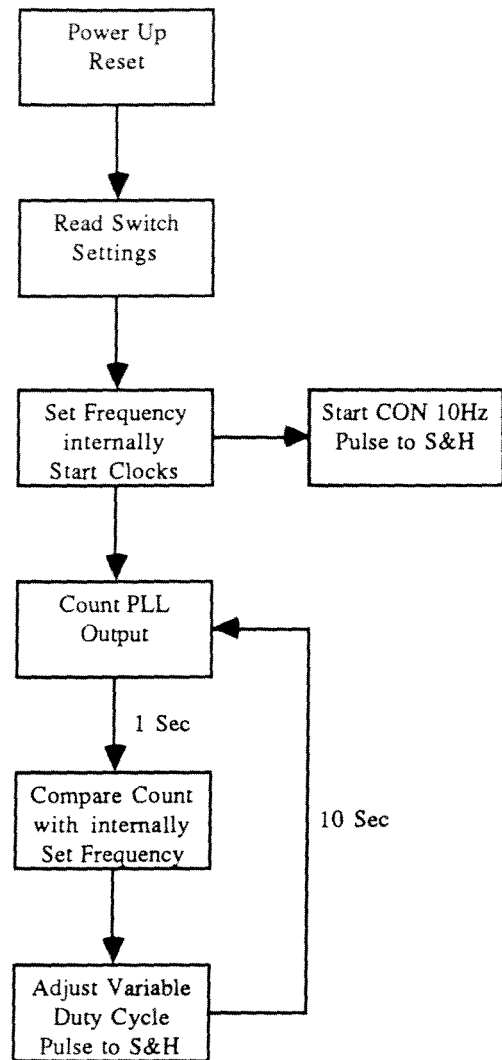
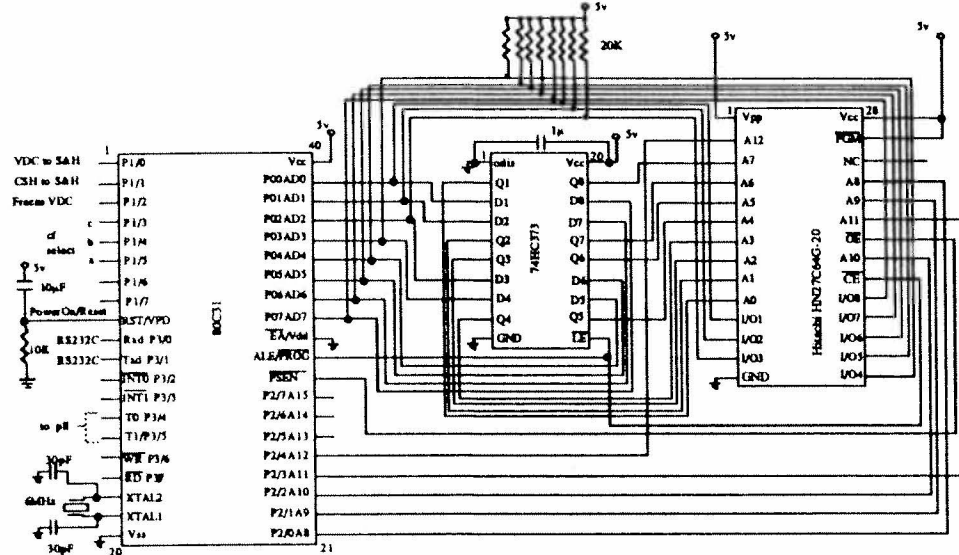
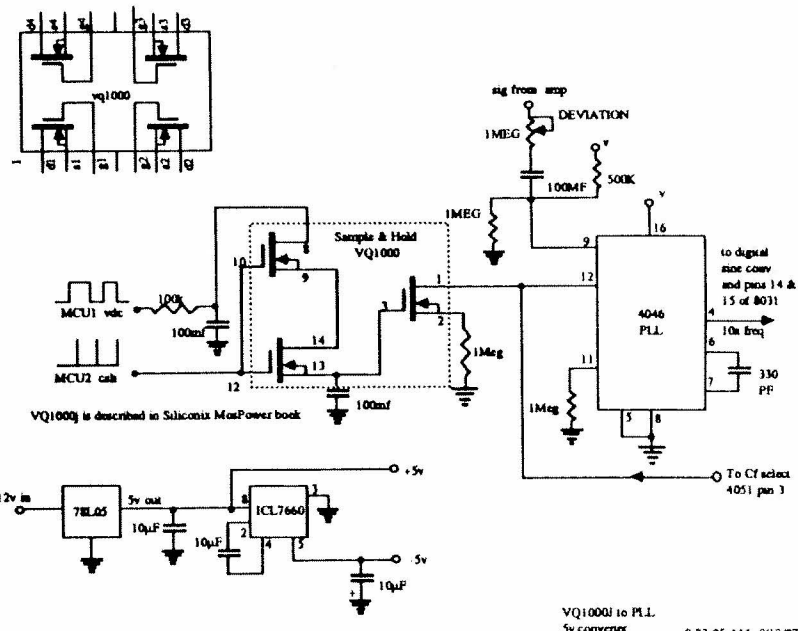


Figure I-4 Logic flow diagram for the new UofW frequency stable VCO design.

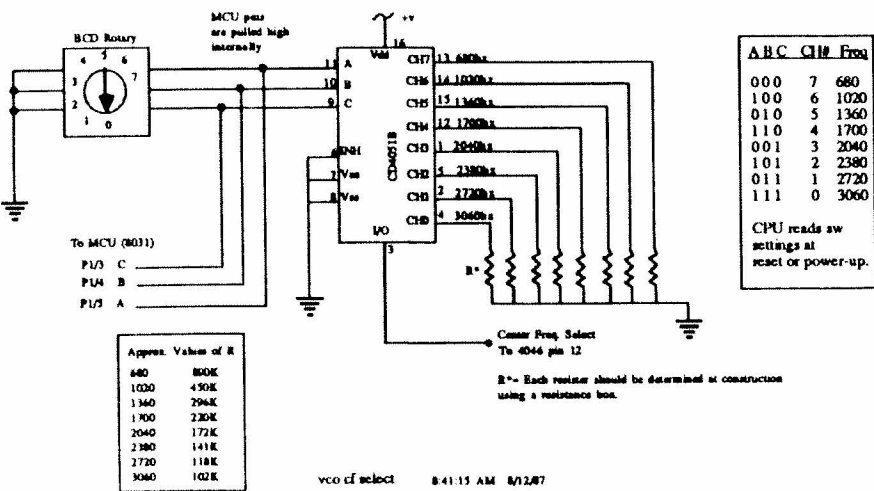
Intel 80C31 MCU to Hitachi HN27C64-20 EPROM



S&H to PLL----5V regulator and -5v converter



VCO Center Frequency select



Sine wave converter to Output

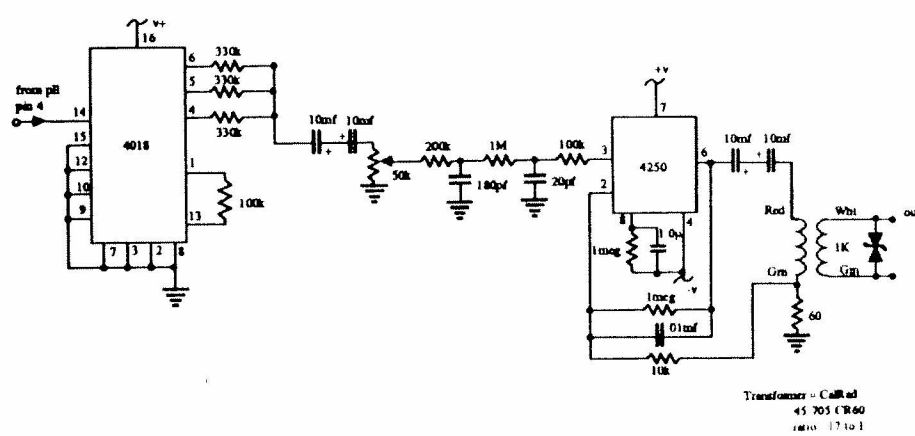


Figure I-5. Schematic diagram and board layout for the new UofW frequency stable VCO.

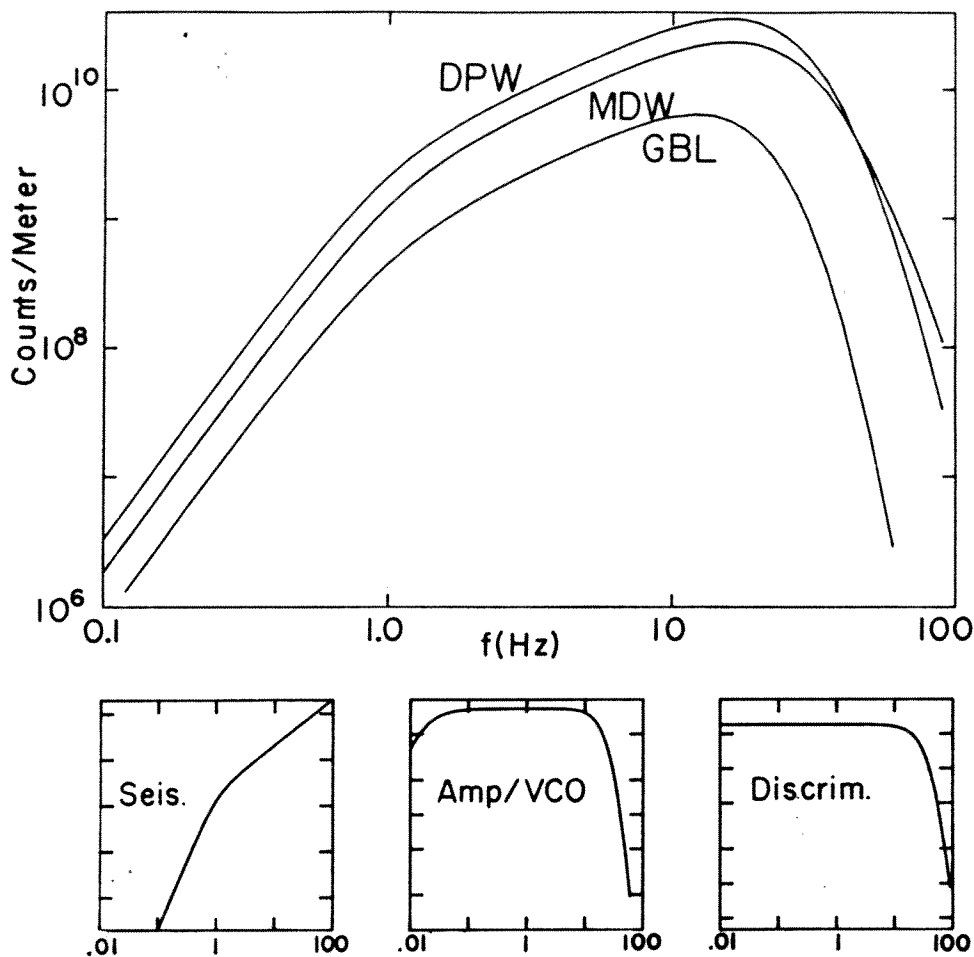
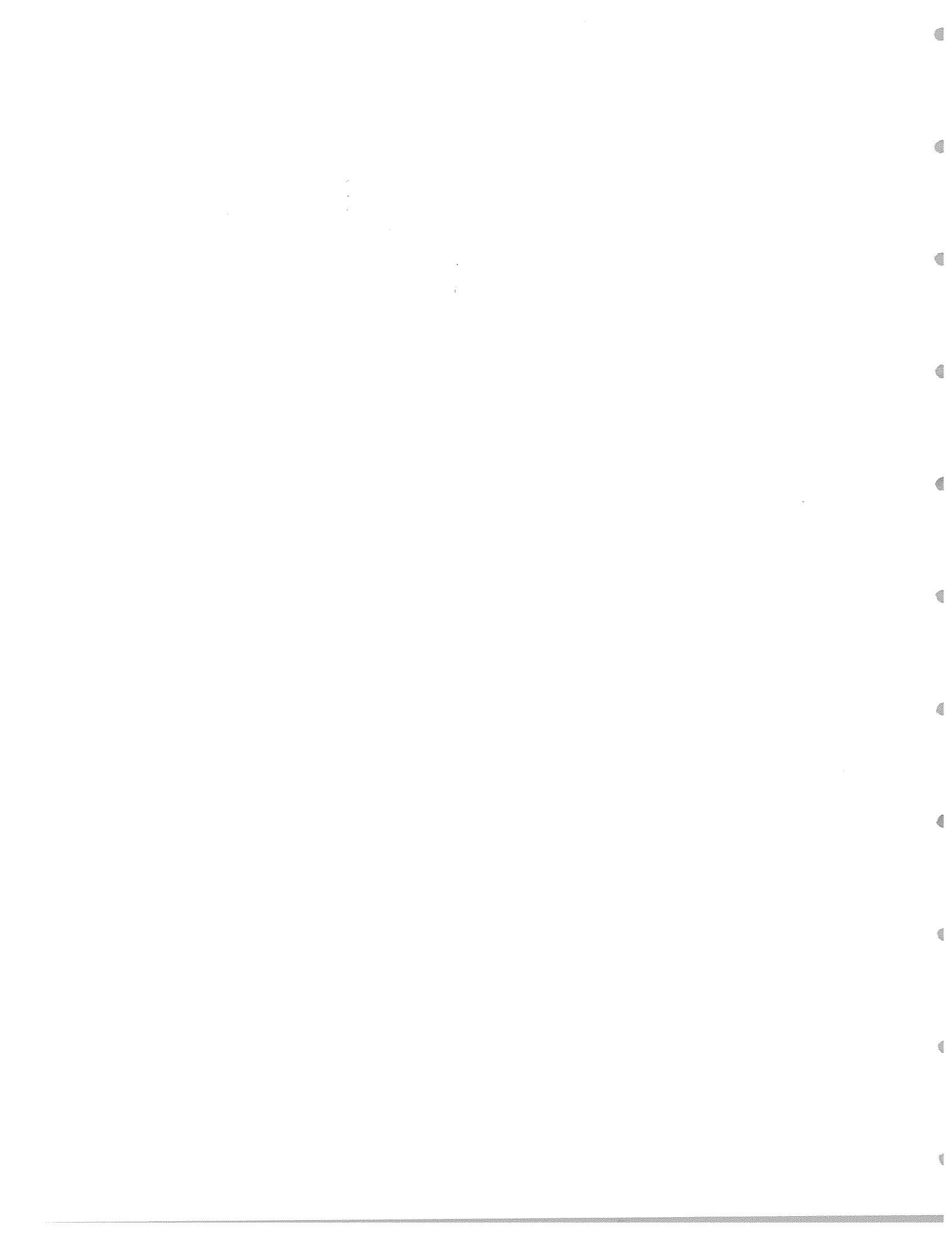


Figure I-8. Frequency response of selected, calibrated stations in eastern Washington. All axes are logarithmic. The small graphs at the bottom show relative frequency response of typical seismometers (volts-sec/m), amplifier/VCO's (Hz/volt) and discriminators (volt/Hz). The overall response of the entire seismograph system is shown for stations DPW, GBL, and MDW in the upper part of the figure. The units of response are counts (as recorded by the DEC 11/34) per meter of ground motion. Stations ETW and GL2 have a response nearly identical to that of GBL. When the digital data are displayed in analog form (*punts*) at a standard scale factor of X1, the stations have ground-displacement magnifications at $f=1.0$ Hz of 271K (DPW), 160K (MDW), 57K (ETW and GBL), and 54K (WA2).



SEISMICITY JULY 1, 1986 - JUNE 30, 1987**Introduction**

From July 1, 1986 to June 30, 1987 we processed 2119 seismic events recorded by the state-wide seismograph network. In eastern Washington and northern Oregon between $44.0\text{--}49.0^{\circ}\text{N}$ and $117.0\text{--}121.5^{\circ}\text{W}$ we located 192 events identified as earthquakes (Figure II-1) and 44 confirmed or probable blasts (Figure II-2).

The largest earthquake in Washington or northern Oregon during the year was a M_c 3.5 event located 63 km deep between Whidbey and Camano islands in western Washington. Eastern Washington earthquakes were generally small; only two had magnitude 3 or greater. All earthquakes and blasts located in eastern Washington or northern Oregon for the year are listed in a catalog as Appendix I of this report. Blasts are distinguished from earthquakes by telephone inquiry or by identifying their characteristic source locations and recorded waveforms.

Seismicity

In general, the distribution of earthquake epicenters for 1986-87 was similar to the distribution in the preceding year. Numerous earthquakes occurred throughout the year near Entiat and many earthquakes occurred in a broad east-west zone along the Saddle mountains. The latter included a tightly clustered swarm of more than forty shallow earthquakes that occurred in September and October, 1986 near Beverly, south of Vantage along the Columbia river. A number of earthquakes occurred at the east end of the Saddle mountains just northeast of the Hanford reservation. One of these was the largest earthquake of the year in eastern Washington, a 14 km deep, M_c 3.4 event on September 1, 1986.

The region northwest of Yakima continued to have earthquakes as in previous years; the largest was a M_c 3.0 earthquake on June 11, 1987 near Naches. The Yakima reservation east of Mount Adams was active again with scattered earthquakes which

filled a region that was without earthquake activity last year. The usually active region southwest of Grand Coulee was fairly inactive this year. Elsewhere in eastern Washington and northeastern Oregon earthquakes were scattered except for a cluster of earthquakes which occurred northwest of Glacier peak (northeast of Darrington) in the fourth quarter of 1986.

Fault plane solutions for the two largest earthquakes of the year, the September 1, 1986 M_c 3.4 earthquake at the east end of the Saddle mountains and the June 11, 1987 M_c 3.0 earthquake near Naches are shown in figure II-3. Both earthquakes were relatively deep (14-17 km) and both fault plane solutions indicate a thrust fault mechanism on nearly east-west trending faults.

Catalog Update

Regional network-type stations have been running in Washington State since 1969. This network has expanded and evolved over these past 18 years both in large steps as well as slow changes. One of the largest changes occurred in 1980 with the beginning of on-line computer digital recording as well as network expansion into the Mount St. Helens area as well as other parts of southern Washington and northern Oregon. All seismic data since 1980 has been processed by the same techniques; the same location routines, velocity models and picking routine has been used on all of these data. Prior to 1980 different techniques, including location programs were used at different times for different parts of the network. The catalog we have been using (computer files: ~ seis/loc.*) and distributing to interested parties has included these nonuniform processed data for the years 1969-1979.

Recently, we have gone back and reprocessed all of these older data using the same programs and velocity models that have been used for all data since 1980. We now have a catalog which goes from 1969 through the present which is the result of uniform processing. The reduced data itself can not be considered uniform over the entire period since the network configuration has changed, as well as the recording and picking

techniques. For example, between 1969 and 1971 the USGS (operators of the eastern Washington Network) picked trace amplitudes rather than coda length for the determination of earthquake magnitude. We have recalibrated their relationship between amplitude and coda length magnitude to try and make a more uniform catalog (Annual Technical Report, 1986).

The current University of Washington earthquake catalog (stored on our computers and available either in computer readable form or in listings as of November 1, 1987) is now updated with uniform processing applied to all data. This means that the location program *spong* and the velocity models (See table II-1) E3, N3, C3, P3, and S3 were used for all data from 1969 to the present. Locations and magnitudes for events reported in previous catalogs and Annual Technical Reports have all slightly changed and thus an exact one-to-one correspondence of maps, tables or catalogs using the current uniform catalog compared to the older ones will not occur.

A brief comparison of the locations from the previous version of the catalog with those of the current uniform catalog is interesting. The most difficult period of time to bring up to the current standard of uniformity is the period 1969-1974. During this period the eastern Washington network was operated by the US Geological Survey and consisted of stations mostly located in the central Pasco Basin. Our previous catalog for this part of the network and this period of time was produced in 1979 (Appendix to Annual Technical Report 1979) by taking the USGS reduced data (arrival times) and using the program *HYP071* and the velocity models then in use in eastern Washington. Magnitudes were primarily those reported by the USGS for the 1969-1971 period and recomputed coda-length magnitudes for 1972-1974. For the current version of the catalog we have gone back to the original USGS reduced data and reprocessed it all using our current location routine and models.

Comparing our previous catalog with the current uniform one shows the following problems and/or differences:

- There were 1549 events in the old catalog and 1541 events in the new one. All events match one to one accept the eight missing events, each of which was labeled a blast in the old catalog. Header cards for these events existed in the USGS reduced data, but no arrival time information. These events have been removed.
- Several (8-10) events had different reference times indicating either a mistake in previous conversion or a mistake that had since been corrected. We have used the reference time in the old catalog.
- Obvious bad picks or coda lengths were found in several (6) of the original data files and were corrected. These were usually obvious typos where data had been placed in the wrong column.

The 1541 events from this period were run through a program to compare differences between the old and new catalogs. 87% of the events in the new catalog located within 2km of their location in the old one. Only four events had greatly differing epicenters ($>8\text{km}$), all of which were earthquakes quite some distance outside the network. 83% of the events in the new catalog located within $\pm 2\text{km}$ of the same depth as those in the old catalog. The new catalog has depths an average of 0.9km deeper than the old, primarily reflecting the fact that fewer events had their focal depths fixed near the surface. A total of 14 events had large differences in depth ($>12\text{km}$), again, mostly events well outside the network or with few stations and no S-picks. The RMS values of the new catalog are about 0.01 seconds larger than those of the old catalog. The values for the standard error in location is an average of 2.6km larger in the new catalog than the old, though this parameter is calculated by a different technique now and thus this difference is not significant. Magnitudes in the new catalog are an average of 0.2 magnitude units lower than those in the old catalog, primarily reflecting the reduction in magnitude during the years 1969-1971 due to the recalibration of the amplitude magnitudes to coda-length magnitudes.

In general the changes in the catalog due to this reprocessing are not large. We do not expect that interpretations or conclusions based on studies using the old catalog need to be modified in light of the reprocessing. It is our hope that this attempt to make the whole catalog more uniform will make future studies of eastern Washington seismicity easier to accomplish with less need to account for apparent changes in seismicity over time that may be due entirely to changes in processing techniques and programs.

Catalog 1986-1987

Appendix I is a catalog of located events between July 1, 1986 and June 30, 1987 in eastern Washington and northeastern Oregon (Fig. II-1 and II-2). The locations reported in the catalog have been determined using the computer program *spong*, which is an adaptation of a program originally written by Bob Herrmann at Saint Louis University. There is a special depth adjustment algorithm in the program for events with poorly controlled locations or depths. Section V of this report is a comparison of this location routine with two other similar routines used widely by seismologists. As shown in figure I-1, different seismic velocity models are used to locate earthquakes in different regions. Table II-1 lists the parameters used for velocity models in each region. Small time corrections are also used at each station but these are not listed in the Table. In each column of the Catalog the following information is given:

- TIME** Origin time is calculated for each earthquake on the basis of multistation arrival times. Time is given in **Coordinated Universal Time** (UTC), in hours:minutes:seconds. To convert to Pacific Standard Time (PST) subtract 8 hours, or to Pacific daylight time subtract 7 hours.
- LAT** North latitude, in degrees and minutes, of the epicenter.
- LONG** West longitude, in degrees and minutes, of the epicenter.
- DEPTH** The depth, given in kilometers, is usually freely calculated from the arrival-time data. In some instances, the depth must be fixed arbitrarily to obtain a convergent solution. Such depths are noted by an asterisk (*) in the column immediately following the depth. A \$ or a # following the depth mean that the maximum number of iterations has been exceeded without meeting convergence tests and both the location and depth have been arbitrarily fixed.
- MAG** Coda magnitude, M_c (Crosson, R.S., 1972, Bull. Seism. Soc. Am., v. 62, p. 1133-1171) For tectonic earthquakes in Washington, M_c is an estimate of local

Richter magnitude, M_L (Richter, C.F., 1958, Elementary Seismology, W.H. Freeman and Co.). Where blank, data were insufficient for a reliable magnitude determination. Normally, the only earthquakes with undetermined magnitudes are very small ones. Magnitude values may be revised as we improve our analysis procedure.

- NS/NP** **NS** is the number of station observations, and **NP** the number of P and S phases used to calculate the earthquake location. A minimum of three stations and four phases is required. Generally, more observations improve the quality of the solution.
- GAP** Azimuthal gap. The largest angle (relative to the epicenter) containing no stations.
- RMS** The root mean square residual taken about the mean of the station first-arrival residuals. It is only useful as a measure of the quality of the solution when five or more well distributed stations are used in the solution. Good solutions are normally characterized by **RMS** values less than about 0.3 sec.
- Q** Two **Quality factors** indicate the general reliability of the solution (**A** is best quality, **D** is worst). Similar quality factors are used by the U. S. Geological Survey for events located with the computer program HYPO71. The first letter is a measure of the hypocenter quality based on travel time residuals. For example: **A** quality requires an **RMS** less than 0.15 sec while an **RMS** of 0.5 sec or more is **D** quality (estimates of the uncertainty in hypocenter location also affect this quality parameter). The second letter of the quality code depends on the spatial distribution of stations around the epicenter, that is, number of stations, their azimuthal distribution, and the minimum distance (**DMIN**) from the epicenter to a station. Quality **A** requires a solution with eight or more phases, **GAP** $\leq 90^\circ$ and **DMIN** \leq (5 km or calculated depth of earthquake, whichever is greater). If the number of phases, **NP**, is five or less, or **GAP** $> 180^\circ$, or **DMIN** $>$ 50 km, the solution is assigned quality **D**.
- MOD** The crustal velocity model used in location calculations (refer to Figure 1).
- P3** - Puget Sound model
 - C3** - Cascade model
 - S3** - Mount St. Helens model including Elk Lake
 - N3** - northeastern model
 - E3** - southeastern model
- TYP** Earthquake classification.
- F** - earthquakes reported to have been felt
 - P** - probable explosion
 - L** - low-frequency earthquakes
 - H** - hand-picked from helicorder records
 - X** - known explosion

TABLE II-1 Current Velocity Models

Velocity models in regions shown in figure I-1. P-wave velocity, V in each layer is assumed constant. S-wave velocity is assumed to be 0.577 times that of the P-wave. Depth is the distance from the earth's surface (reference plane) to the top of each layer.

Southeast (E3)		Northeast (N3)	
V (km/sec)	Depth (km)	V (km/sec)	Depth (km)
3.70	0.0	5.1	0.0
5.15	0.4	6.1	0.5
6.10	8.5	6.4	14.0
6.40	13.0	7.1	24.0
7.10	23.0	7.9	38.0
7.90	38.0		

Cascade (C3)	
V (km/sec)	Depth (km)
5.1	0.0
6.0	1.0
6.6	10.0
6.8	18.0
7.1	34.0
7.8	43.0

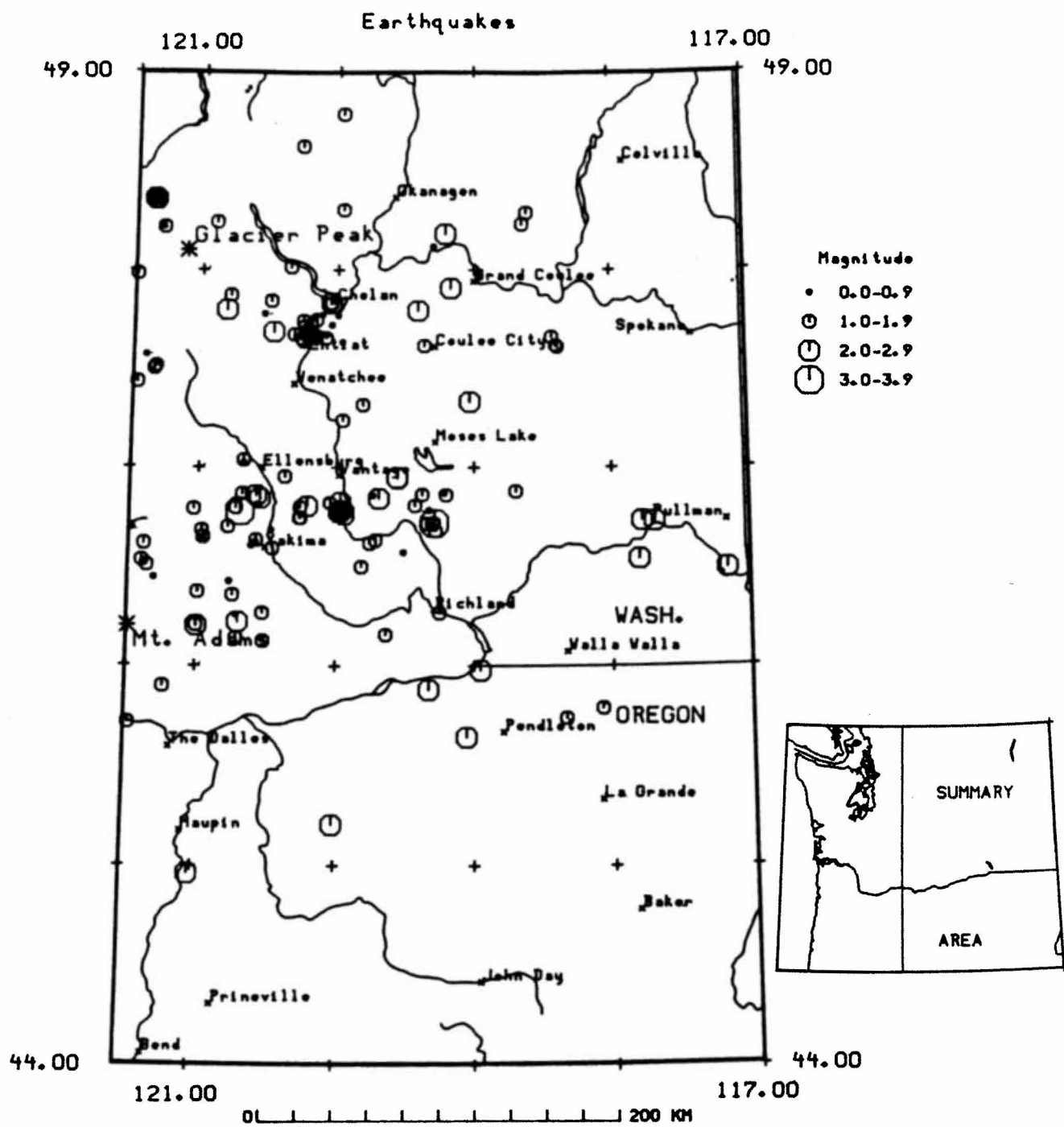


Figure II-1. Earthquakes in eastern Washington and northeast Oregon, July 1, 1986 - June 30, 1987. The boundary of the Hanford reservation is shown near the center of the map. The area summarized in this report is shown at lower right.

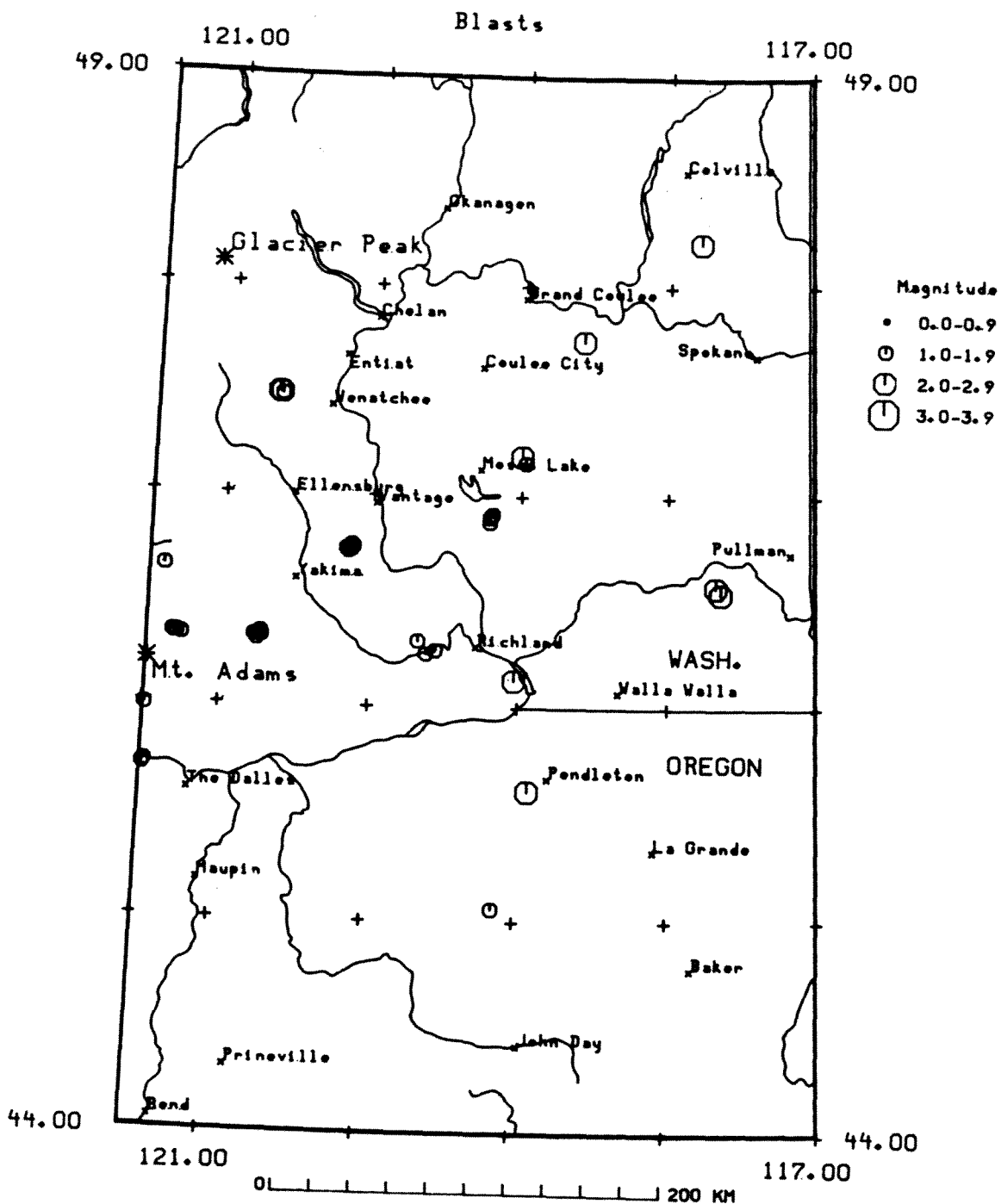
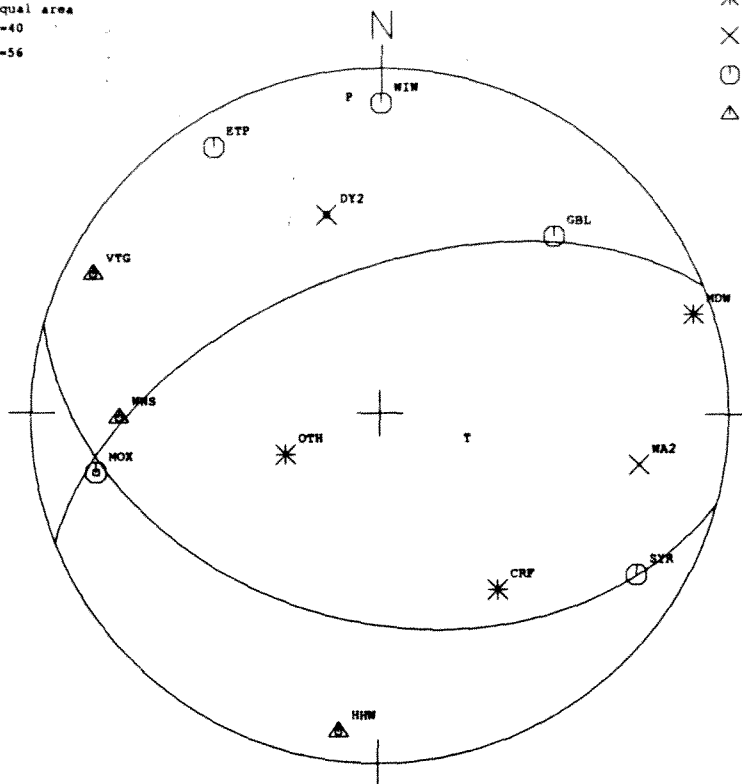


Figure II-2. Known or suspected blasts in eastern Washington, July 1, 1986 - June 30, 1987.

A 8609012132 43.96 46N4311 119W1711 14.09 3.4 18/019 81 5 0.09 0.4AA E3
 Velocity model: V0= 5.1, DV= 0.08

Lower hemisphere equal area
 Azimuth=195 Plunge=40
 Azimuth=338 Plunge=56
 P az=354 P pl= 9
 T az=107 T pl=69
 fp-fit 0.09 AIA

* = 'C'
 X = 'P'
 O = 'D'
 △ = 'T'



A 8706111950 16.98 46N4665 120W4164 17.23 3.0 33/042 29 11 0.35 1.0CA E3
 Velocity model: V0= 5.1, DV= 0.08

Reversed stations: WEN TWN
 Lower hemisphere equal area
 Azimuth=185 Plunge=35
 Azimuth= 5 Plunge=55
 P az= 5 P pl=10
 T az=185 T pl=80
 fp-fit 0.00 AIA

* = 'C'
 X = 'P'
 O = 'D'
 △ = 'T'

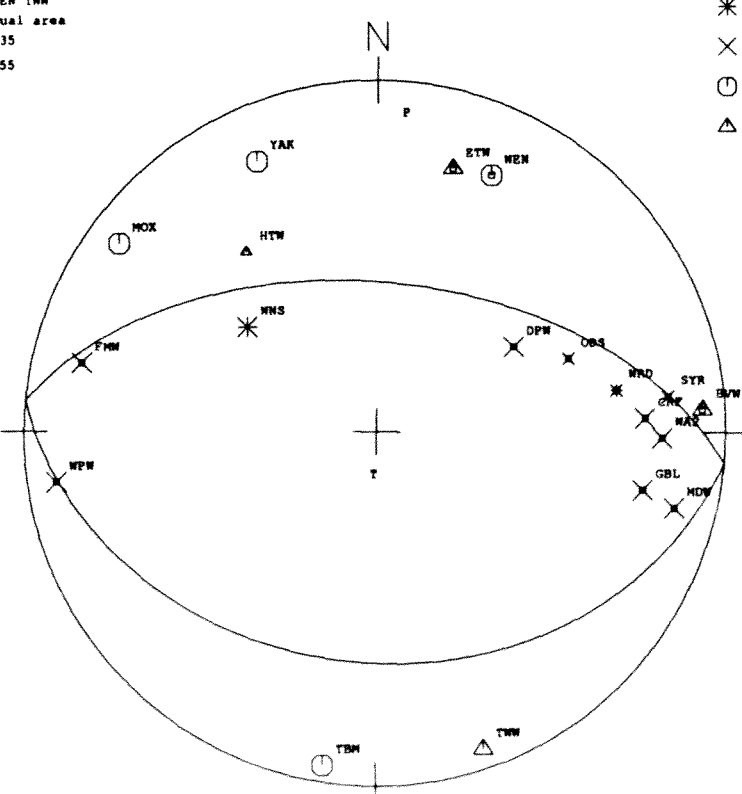


Figure II-3. Focal mechanism solutions for two larger events in eastern Washington during the past year. The upper plot is for the event on Sep 1, 1986 at 21:32Z located at $46^{\circ} 43' N$ $119^{\circ} 17' W$ at a depth of 14.1km, $M=3.4$. The lower plot is for the event on Jun 11

III - FOCAL MECHANISM SUMMARY

Introduction

Since the installation of the first micro-earthquake type network in 1969 in the Hanford area 3795 earthquakes have been recorded and located in eastern Washington. Out of all of these events, only a few have had focal mechanisms determined because of a number of reasons. Most of the events are simply too small to be well enough recorded for the unambiguous determination of first motion polarities at very many stations. For some of the large events station distribution around the focal sphere is not uniform enough to allow for anything other than a very poorly controlled mechanism determination. However, in each of the past several years we have reported focal mechanisms for several larger earthquakes. These mechanisms were determined by hand after careful review of the first motion data.

The results of these previous studies show a general pattern of consistent orientation of the major compressive stress axis (P) in the horizontal north-south direction, while the minimum compressive stress axis (T) varies from vertical to east-west. Other than this general observation no other distinctive pattern has been observed. We are now starting a program of systematically reviewing polarity data and determining mechanisms to develop a comprehensive catalog of focal mechanisms for eastern Washington.

During the past year we have implemented two different automatic focal mechanism determination routines and have begun applying these procedures routinely as events are processed. We have also begun reanalyzing earthquakes from the past eight years using these routines.

Mechanism Determination Procedures

Both of these routines use a search algorithm for fitting a double-couple type mechanism to weighted first motion data. One routine is *sppfit* by Reasenberg and

Oppenheimer¹, the other is *focplt*, a program written by Whitcom and Garmany in 1971, and modified by Jim Pechmann of the University of Utah. These routines have been compared to one another by running the same data through each and comparing results. Both programs search the focal sphere for solutions and plot the "best" fitting solution. Both display the azimuth and plunge of the slip vectors of the fault and auxiliary planes, and the P- and T-axes. A measure of the confidence level of the fit is also given. If more than one solution has a required degree of confidence, then alternate planes may also be represented on the focal sphere.

Fpfit uses a two-stage grid search procedure that finds the source model minimizing a normalized, weighted sum of first-motion polarity discrepancies. Two weighting factors are incorporated in the minimization; one reflecting the estimated variance of the data, and the other based on the absolute value of the theoretical P-wave radiation amplitude. The latter weights down observations near radiation nodal planes.

Focplt also searches the focal sphere, but after testing for all possible solutions *focplt* determines the "best" solution by placing one slip vector in the middle of the most well-constrained slip vector minimum, and the other as close to the centre of the other slip vector minimum as possible. Output from *focplt* is in a similar form to *fpfit* though the nodal planes are described in terms of their azimuth and dip. In addition *focplt* creates an output text file containing information about the slip vectors, and the P- and T-axes, showing their range on the focal sphere. Input and output data, and rake and plunge calculations for the nodal planes are also summarized here.

A Comparison of Fpfit and Focplt

The focal mechanism solutions of 17 events chosen from the our catalog for years 1980-1986 were calculated using both fitting routines *fpfit* and *focplt*. All the earthquakes were from the Puget Sound and Mount St. Helens area, and had a minimum of

Reasonberg, P. and D. Oppenheimer *FPFIT, FPPLLOT, FPPAGE: Fortran computer programs for calculating and displaying earthquake fault-plane solutions*, Open-File Report No. 85-739, 1985

10 P-wave first-motion polarities. For each event the number of polarities, the position on the focal sphere of the P and T axes, and the number of stations that were inconsistent with a focal mechanism solution (compression or dilatation in the wrong quadrant, *err*) are shown in Table III-1.

Table III-1 Comparison of Fpfit and Focplt Solutions

Event	# sta	FPFIT						FOCPLT							
		P-axis		T-axis		err	P-axis		T-axis		az	dip	az	dip	err
		az	dip	az	dip		az	dip	az	dip					
800519	17	010	24	227	60	1.0	010	21	221	65	1.0				
810214	47	205	11	114	03	7.5	210	23	112	20	4.0				
810214	59	045	90	315	0	6.0	087	02	042	02	6.0				
810513	55	016	11	284	11	2.5	014	04	286	11	2.5				
810513	37	006	24	264	24	3.5	016	19	268	43	2.0				
830812	24	154	15	038	59	1.5	155	17	036	56	1.5				
831031	38	310	75	130	15	0.0	326	74	132	17	0.0				
831204	26	189	13	286	28	1.0	200	02	101	03	0.5				
840408	32	284	22	044	51	1.5	288	21	042	49	1.5				
850228	35	319	29	110	58	1.0	313	29	110	60	1.5				
851117	27	239	11	331	11	1.0	223	68	327	59	0.5				
851122	17	015	00	105	90	0.0	013	12	280	12	0.0				
860603	12	017	06	115	53	0.0	213	89	303	70	1.0				
860708	39	315	63	078	16	3.0	337	70	075	04	3.0				
860831	20	177	55	057	19	1.0	170	39	053	29	2.0				
861020	20	215	10	35	80	2.0	207	06	358	81	1.0				
861021	18	010	16	222	71	0.0	009	21	219	66	0.0				

*err- weighted number of stations in error.

Fpfit and *focplt* determined the same type of mechanism in almost all cases. Where they sometimes differed, both solutions were consistent with the data (ambiguous determination because of poorly distributed data). Figure III-1 illustrates a comparison of *fpfit* and *focplt* for an earthquake with less than the best distribution of first-motion data. Two almost equally valid solutions are produced by *fpfit*, one of which is not greatly different than the solution from *focplt*. *Fpfit* purposely tries to find non-pure strike-slip solutions since strike-slip solutions are the easiest for an analyst to recognize by hand.

Nine of the 17 events had solutions where the P- and T-axes were within 6 degrees of each other in both azimuth and plunge. The axes of fifteen of the events differed by less than 16 degrees. From a count of "stations in error" over the 17 events *fpfit* had a

slightly worse record than *focplt*, but the difference is not significant (*fpfit*=32, *focplt*=28). Both routines find "good" solutions, usually within a few degrees of each other, when the polarity pattern on the focal sphere is well-distributed. Where the mechanism is poorly constrained *fpfit* may determine more than one set of nodal planes. *Focplt* calculates an average solution, and hence doesn't always minimize the number of stations in error. This can be corrected by studying the slip vector plot in the output file.

For determining mechanisms from data with a low number (<10) of P-wave polarities *fpfit* produces solutions that seem to fit the data closer than does *focplt*. From this study we are encouraged that, in the majority of cases, the solutions determined by *fpfit* and *focplt*, are indistinguishable within the error bounds of the calculations. We have chosen to use the *fpfit* program for our routine automatic determination of mechanisms since the error estimates it provides are more compatible with our representation system for location quality of events. For example *fpfit* returns quality indicators of **A**, **B**, and **C** meaning good, medium, and poor solutions, respectively. It also computes estimates of the uncertainty in the model parameters and a graphical illustration of solutions within these uncertainties.

Data and Analysis

We have begun our review process of focal mechanisms with data recorded digitally on the on-line computer system since 1980. These data have more reliable first motion picks and are easier to check than the pre-1980 events which were recorded only on film. We plan to include older data in this summary in the future.

Our data selection process is to first, search for all events which have locations east of 121.5 and have eight or more first-motion picks. From this set we exclude events which have no station closer than 20km and which have azimuthal gaps greater than 120°. There were 227 events which met these criteria. These events were then processed by the program *fpfit* and the resulting mechanisms plotted for visual examination.

For almost half of these events no solution, or a very poorly constrained solution was obtained. This was primarily due to poor sampling of the focal sphere. Of the 123 events with solutions, 88 were well enough determined to study in detail. Some of the others may also be useful to study after repicking first motions from the original trace data. Of the 88 good solutions, trace data for those events for which there were inconsistent first-motions or which had poorly controlled mechanisms were re-examined to see if the original picks were possibly in error. Of the 1453 first-motion picks in this whole data set only about 30 have been modified as a result of this preliminary re-examination indicating that most of the original data were in fairly good shape to begin with. Events from the 1981-1982 period had the most problems; a period when analysis procedures were not as well developed as they have been recently. After these corrections, *fpfit* was again run and the results classified as to quality after additional visual review.

Results

There were 35 events with **A**-quality solutions, 35 with **B**-quality, and 18 with **C**-quality. The **C**-quality events are poor enough to not be considered further at this time. Table III-2 lists the important parameters for the **A**- and **B**-quality mechanisms. Figures III-2 and III-3 are summaries of these mechanism solutions.

Table III-2 Mechanism Summary

Date-Time	Lat deg-min	Lon deg-min	Depth km	Mag	P-Axis		T-axis		Q
					Az	dip	Az	dip	
8007280716	48 27.08	120 20.45	9.53	2.4	159	30	58	18	B
8010182339	47 40.24	120 06.12	4.42\$	1.8	309	13	75	69	B
8011090236	47 40.70	120 04.57	8.16	2.7	158	19	5	68	A
8011170725	46 37.07	120 32.30	12.80	1.5	186	0	278	67	A
8012032346	47 41.05	120 08.24	2.82	2.2	214	3	315	74	A
8012182244	45 49.98	120 00.44	0.03*	2.8	5	11	274	3	A
8102020123	46 15.77	120 59.34	1.98*	4.0	186	28	89	13	A
8102132315	47 11.93	120 53.96	7.83	1.6	304	11	36	11	B
8102150813	47 11.83	120 54.33	5.80	2.6	335	45	192	38	B
8102180609	47 11.84	120 53.55	3.37	4.2	8	36	181	54	A
8102191719	46 40.73	119 18.28	0.04*	2.7	162	24	6	64	B
8103061418	47 11.87	120 53.01	0.04*	2.9	7	20	175	69	A
8103102249	47 27.10	121 20.30	8.07	2.6	2	11	115	63	B
8103150723	47 59.24	121 29.58	5.35	3.6	179	15	63	59	A
8105262110	47 39.45	120 17.16	2.74\$	2.6	322	7	219	62	A
8105280855	46 31.80	121 23.91	2.98	4.6	5	7	275	7	A
8105280910	46 31.52	121 23.64	3.22	5.0	11	3	280	11	B
8105291512	47 37.44	119 54.12	1.17*	2.5	265	63	28	16	B
8106141312	45 57.70	120 30.42	13.58	3.2	352	14	140	73	A
8106302032	47 01.42	120 13.30	0.33	2.0	168	2	74	58	A
8107021246	46 31.89	121 23.12	5.41	2.2	9	31	177	59	B
8107021959	46 32.38	121 23.32	6.12	2.4	351	20	124	62	B
8107030834	46 32.53	121 23.37	5.12	2.2	171	3	70	74	B
8107220605	47 46.65	120 17.28	9.53	3.0	143	24	299	64	A
8108061232	46 28.76	121 19.98	4.01	2.8	346	18	252	10	A
8109100006	46 30.96	121 23.02	3.99	2.0	180	17	82	24	B
8109201223	46 08.51	119 27.16	9.64	2.2	157	24	1	64	B
8109231628	46 31.34	119 43.49	19.58	2.3	8	7	272	44	A
8110071210	46 31.27	121 22.53	4.05	2.6	5	41	98	3	B
8110150849	46 58.05	120 26.22	8.74	2.3	4	20	231	62	B
8110250320	47 45.51	120 11.77	7.58	3.2	142	19	262	55	B
8201231531	46 32.77	121 22.67	3.33	3.2	183	35	277	5	A
8202030937	47 03.86	120 58.22	1.41\$	2.5	200	7	107	21	B
8202180327	47 39.84	119 44.70	0.80	2.8	125	15	305	75	A
8202192332	46 31.17	121 22.62	3.10	2.1	171	29	285	37	B
8207181405	46 31.68	121 23.07	6.48	2.9	358	21	265	7	B
8209261009	46 52.04	121 02.86	3.25	3.4	191	23	296	31	A
8210140853	47 42.88	120 11.51	3.87	2.4	311	7	68	76	A
8211080023	46 52.66	119 28.34	13.81	2.3	172	19	325	68	A
8211090235	46 52.89	119 27.97	14.01	2.3	173	24	329	64	A
8211212219	46 52.82	119 27.75	14.47	1.9	160	0	250	90	B
8212141948	47 11.61	120 53.76	0.04*	2.8	358	22	146	64	A
8212200420	46 31.71	121 23.35	5.26	2.7	190	21	283	7	B
8303221247	45 59.52	118 24.18	7.53	3.8	119	14	209	0	B
8305210111	47 16.94	121 24.85	11.69	2.8	168	24	70	17	A
8306101819	47 39.40	120 17.11	4.88	2.7	311	2	48	76	B
8309140902	47 42.97	120 16.30	4.48	2.5	308	7	51	62	B
8310200944	46 43.02	119 35.04	1.86	3.4	6	4	97	18	B

Mechanism Summary (cont)

Date-Time	-Lat deg-min	-Lon deg-min	Depth km	Mag	P-Axis		T-axis		Q
					Az	dip	Az	dip	
8311141118	46 39.32	120 35.99	7.87	3.8	189	13	314	68	B
8312050724	46 54.89	120 42.78	7.76\$	3.8	189	13	286	28	A
8404110307	47 32.10	120 11.13	8.02	4.3	346	14	93	49	A
8406021104	46 39.54	120 35.99	8.08	2.6	193	19	40	68	A
8410100324	47 54.22	119 04.75	15.39	3.0	43	6	305	53	B
8501082356	47 03.36	120 05.61	0.58	2.8	188	15	297	49	B
8501090251	47 03.61	120 05.24	0.65	2.8	158	29	316	59	B
8501090546	47 03.83	120 05.65	0.34	3.3	171	6	273	65	A
8501250728	46 29.99	120 37.93	16.63	3.1	182	5	302	81	B
8501310302	47 03.57	120 05.03	0.29	3.3	172	41	20	46	B
8502102029	45 42.27	119 38.07	18.41	3.9	353	21	260	7	A
8510010525	46 47.78	120 02.87	1.09	3.0	46	15	304	38	A
8510101006	47 44.95	120 15.93	7.04	3.2	106	3	5	74	B
8511221809	47 15.76	119 21.07	20.82	3.2	15	0	105	0	A
8602040158	46 02.64	118 48.60	7.80	3.2	20	30	200	60	B
8603041224	46 55.40	120 39.41	9.81	2.5	201	6	303	65	A
8606201655	46 28.20	120 54.79	3.42	2.8	326	13	229	28	A
8609012132	46 43.11	119 17.11	14.09	3.4	354	9	107	69	A
8609020237	46 43.12	119 17.40	13.49	1.8	145	11	240	24	A
8611081453	46 51.54	120 34.82	8.42#	2.9	32	67	253	18	B
8612080332	45 58.60	118 57.18	19.53	2.6	335	45	165	45	B
8702170939	46 50.63	120 33.21	7.25	2.1	345	7	75	7	B
8706111950	46 46.65	120 41.64	17.23	3.0	5	10	185	80	A

Note that some of these solutions are slightly different than those published in previous annual reports. For example, the solution for the event on 86/03/04 at 12:24 has slightly different strikes for the nodal planes than the solution published last year in the annual report, figure II-3e. The T-axis in this case is also closer to vertical; however, the P-axis remains almost exactly the same. These two solutions as well as one produced by the program *focplt* are shown in figure III-4 to illustrate typical difference between the results of the two automatic programs as well as an independent solution done by hand. Note that the solution produced by *focplt* is very close to that produced by *fpfit* and though the manual solution is a bit different, it fits the data just as well as those produced by the automatic routines. Note that the orientation of P-axis for all solutions are almost the same while the T-axis orientations vary over a solid angle greater than 20° . This is typical of all events with more dilatational arrivals than compressional ones, and is consistent with the error estimates returned by *fpfit* indicating, that for most of the events studied, the P-axis is much better determined than the T-axis.

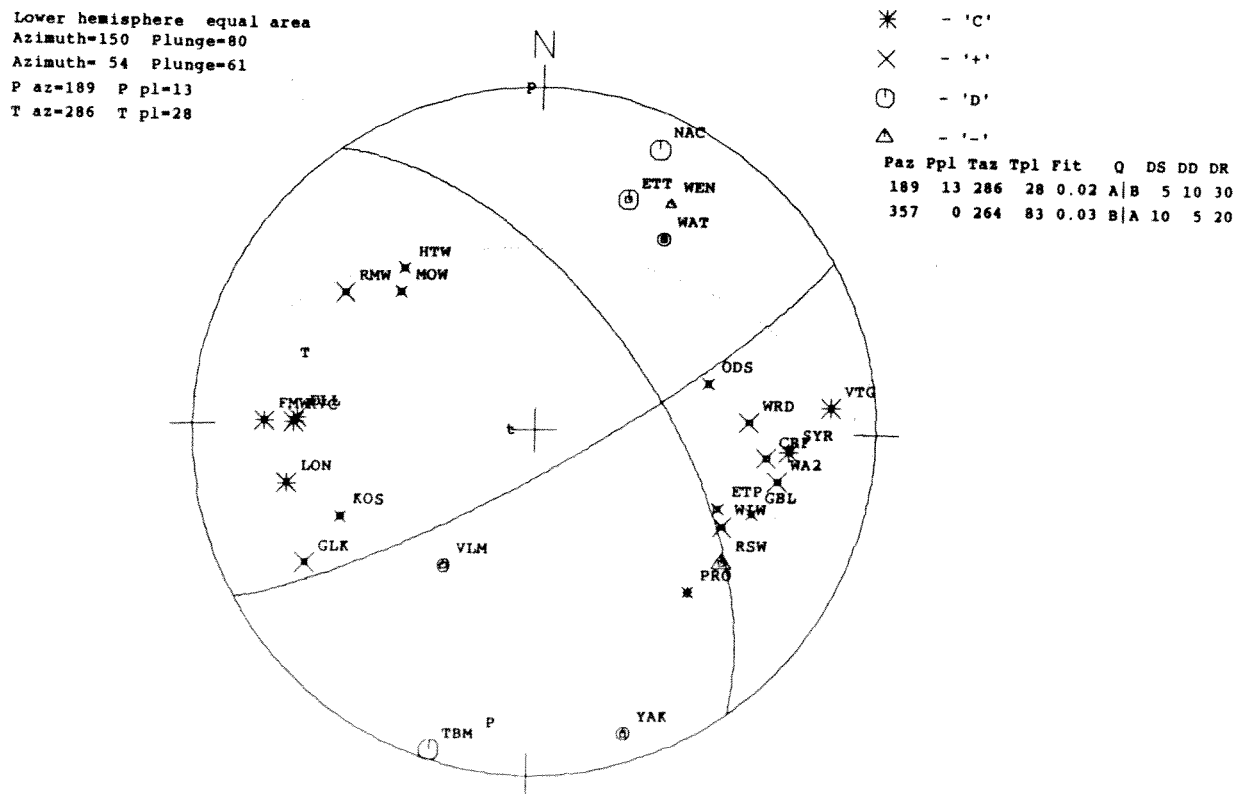
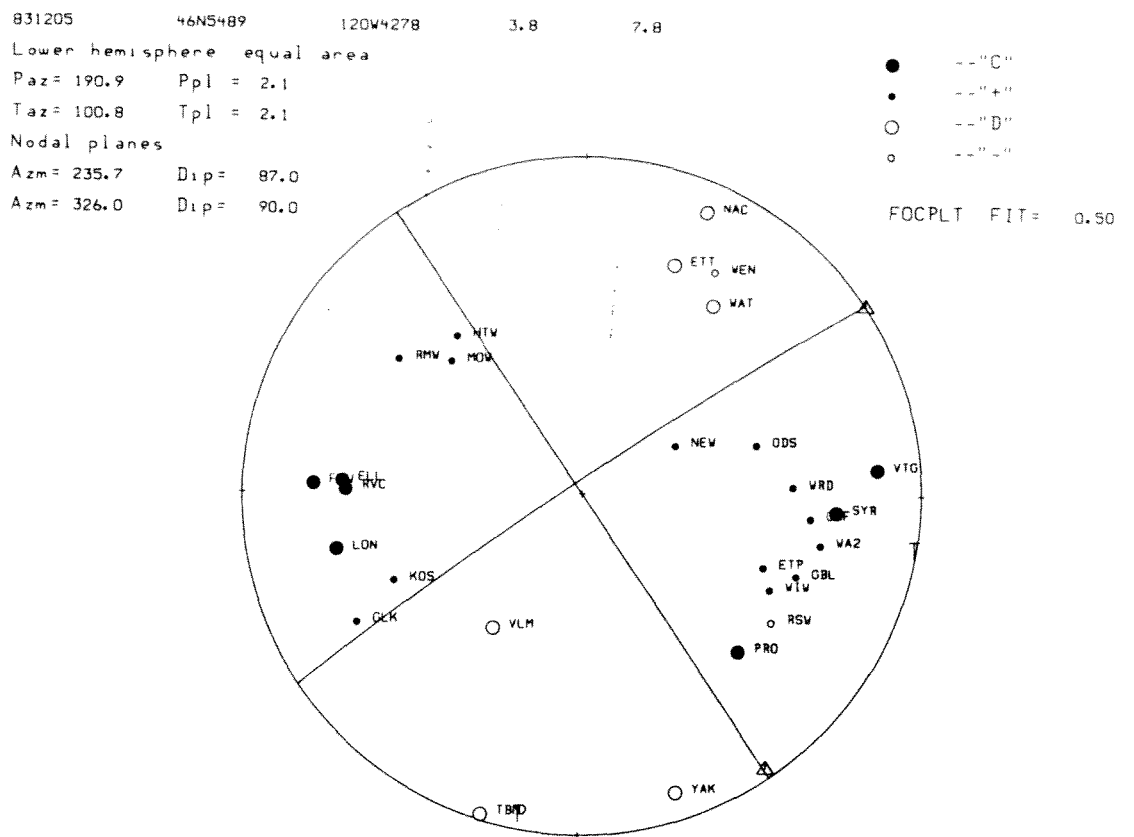
A summary of the orientations of all of the P- and T-axes are shown in figure III-5. This figure supports the general observation previously made that P-axis tend to be oriented in a horizontal, north-south direction, while T-axis tend to be more vertical and swing in a general east-west direction. Note that there seems to be a wider spread, particularly for the T-axis, for the **B**-quality solutions as compared to the **A**-quality ones.

In order to examine the spacial distribution of the mechanisms, we plot the horizontal projection of all P-axis with a dip less than or equal to 30° on a map of eastern Washington in figures III-6 and III-7. This includes 59 of the total 70 **A**- and **B**-quality solutions studied. The **A**- and **B**-quality solutions are separated on figures III-6 and III-7 respectively. Note that, other than for a few inconsistent events, most of the P-axes in one part of eastern Washington have pretty much the same horizontal projection. The P-axis orientations in some areas differ significantly from those in other areas. Notice that for the area just south of Lake Chelan the P-axis orientations are northwest-

southeast with a few oriented almost due east-west. In the Yakima-Ellensburg area most of the P-axis are oriented just slightly east of north while over the rest of southeastern Washington, particularly in the central basin, the P-axis orientations scatter slightly about due north-south.

Filled symbols for events shown in figure III-6 and III-7 represent events with their T-axis within 30° of vertical, that is, almost pure thrust events. The remaining events have a significant proportion of strike-slip component to their mechanisms. Note that in the south Lake Chelan area almost all of these events are nearly pure thrust events. The orientations of the fault and nodal planes are mostly orthogonal to the regional structure, which is dominated by northwest-southeast trending grabens. In the north central basin, many events show nearly pure thrust-type solutions while in the south and the east flank of the Cascades many events tend to have partial strike-slip mechanisms. The tectonic implications of these observations have yet to be determined.

We are continuing our efforts to review the focal mechanisms of eastern Washington earthquakes. Most of the larger events since 1980, ones with many good first-motion picks, have been reviewed. There may be another 20 or so events for which a mechanism may be determined after additional review of original first motion data. We also plan to use the automatic mechanism determination routines for events from the 1970s. Review of first-motion data from these events will be more time consuming since they were recorded on Develocorder film.



Figures III-1. A comparison of the focal mechanism solutions generated by *focptl* (top) and *fpfit* (bottom) for an earthquake on Dec 5, 1983 at 46° 55'N, 120° 43'W and depth of 7.8km, M=3.8. Note that two solutions are shown for *fpfit*, both of which are about equally good.

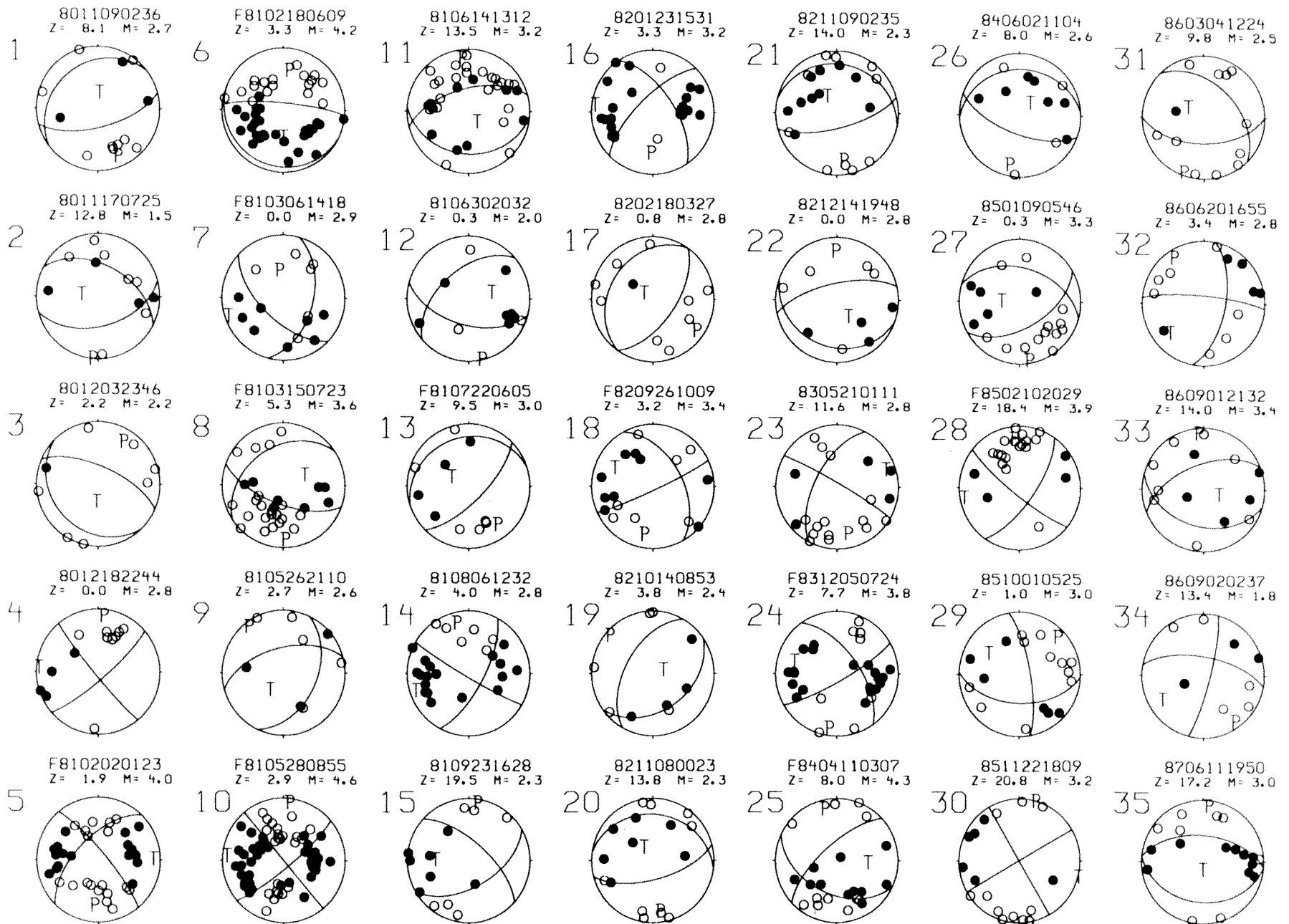


Figure III-2. Summary of the focal mechanism produced by *fpfit* with **A**-quality. The date-time identifier (matches first column in table III-1) is shown above each solution as well as the event's depth and magnitude.

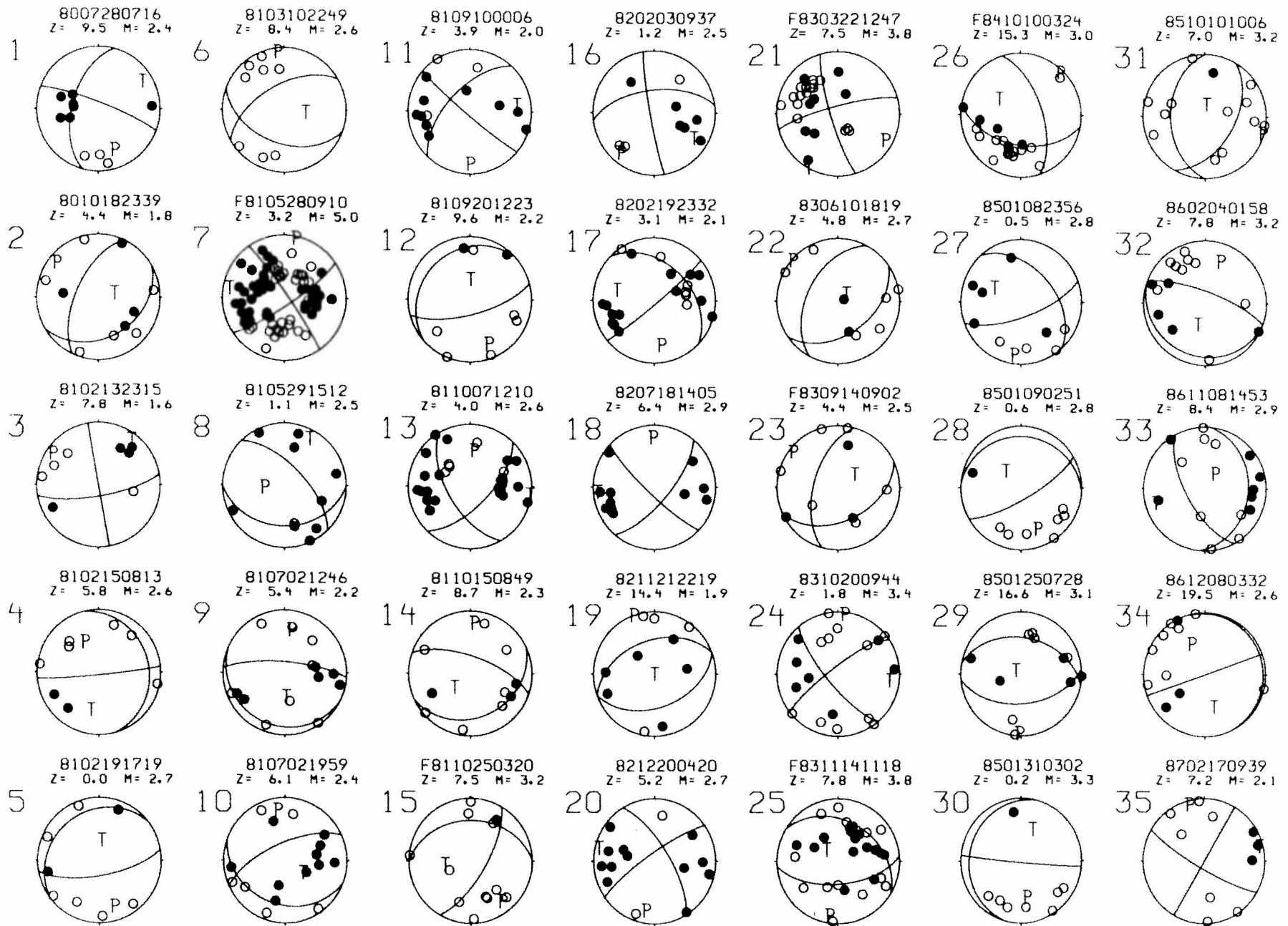


Figure III-3. Summary of the focal mechanism produced by *fpfit* with B-quality. The date-time identifier (matches first column in table III-1) is shown above each solution as well as the event's depth and magnitude.

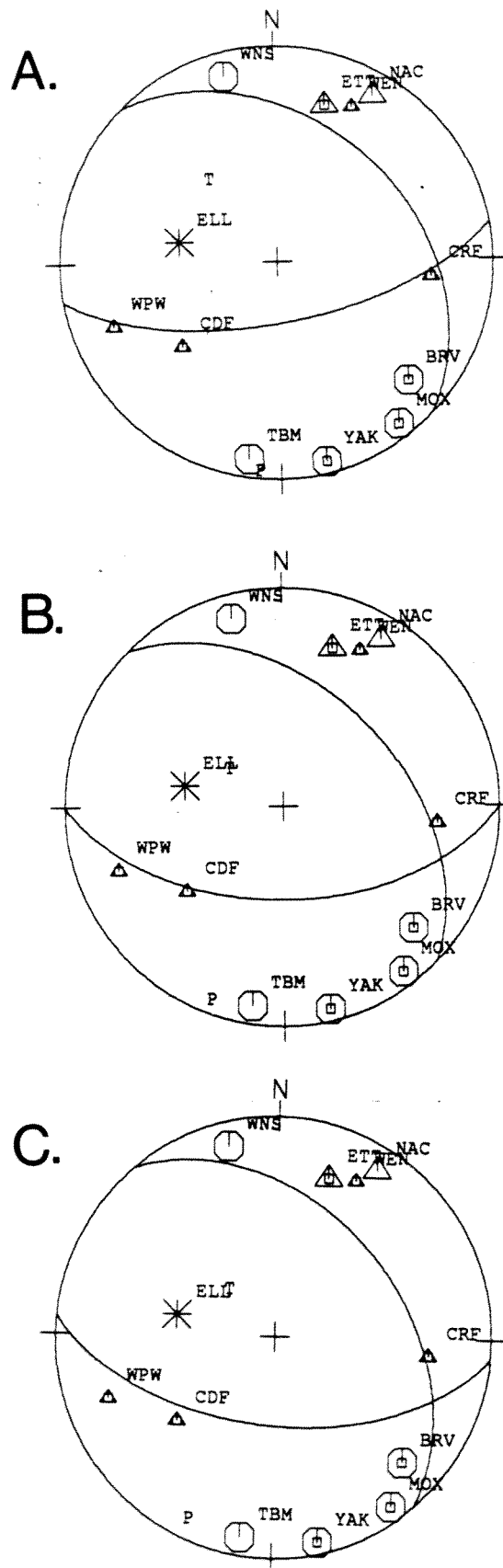


Figure III-4. Comparison of three different focal mechanism solutions produced by three different procedures; A- by hand (from figure II-3e from 1986 Annual Technical Report), B- by *fppfit*, C- by *focplt*.

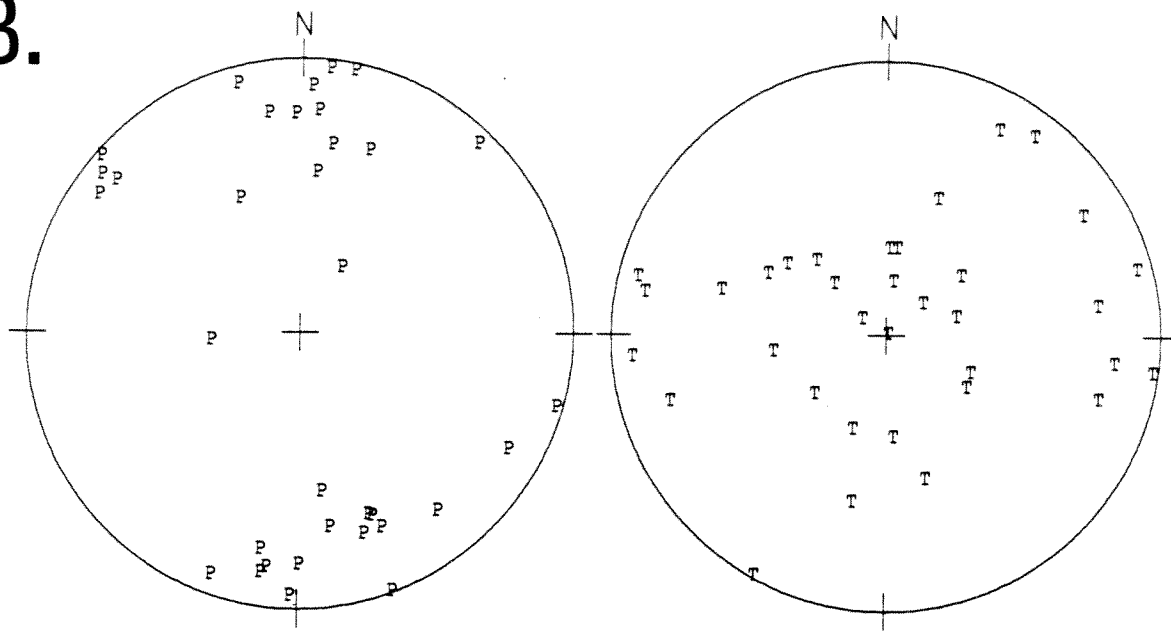
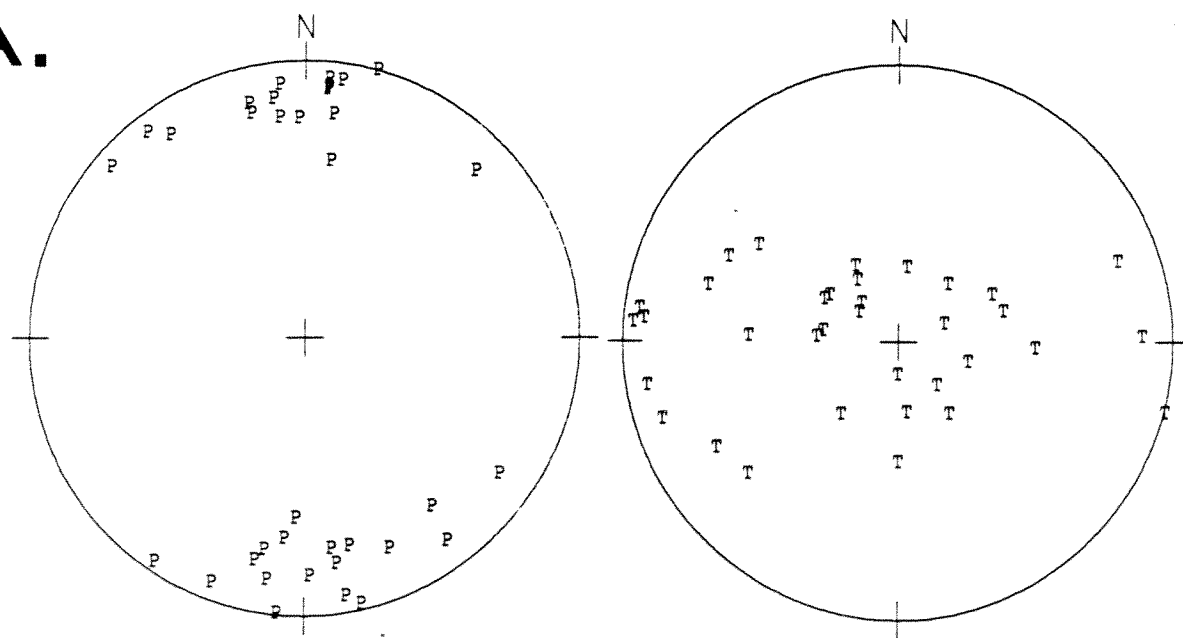
B.**A.**

Figure III-5. Summary of P- and T-axes for A-quality solutions (bottom), and B-quality solutions (top).

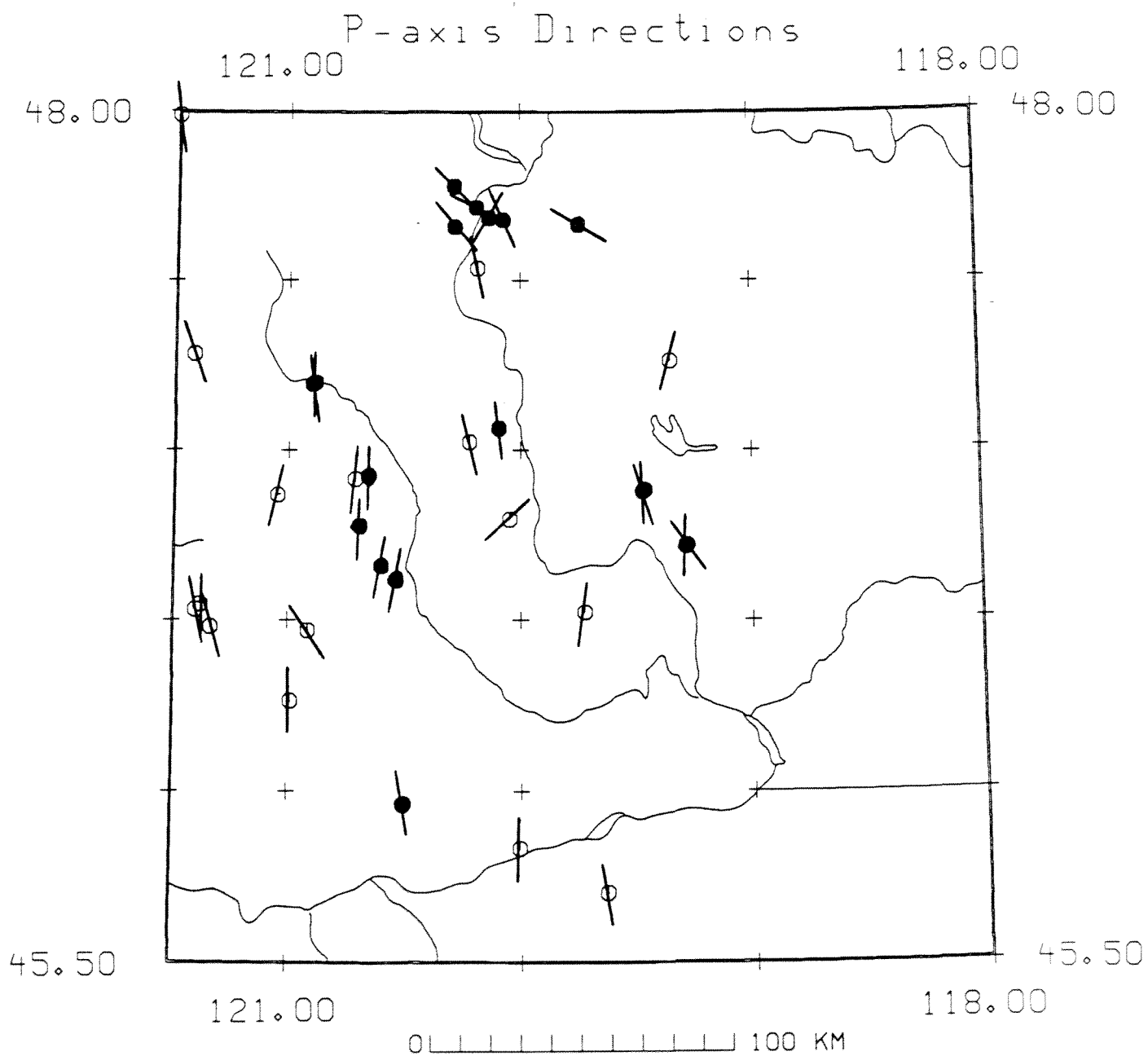


Figure III-6. Summary of orientation of P-axes for A-quality solutions. Events with a P-axis within 30° of horizontal have the horizontal projection of that axis shown as a line. Events whose T-axis is within 30° of vertical have filled symbols. Such events have nearly pure thrust-type solutions

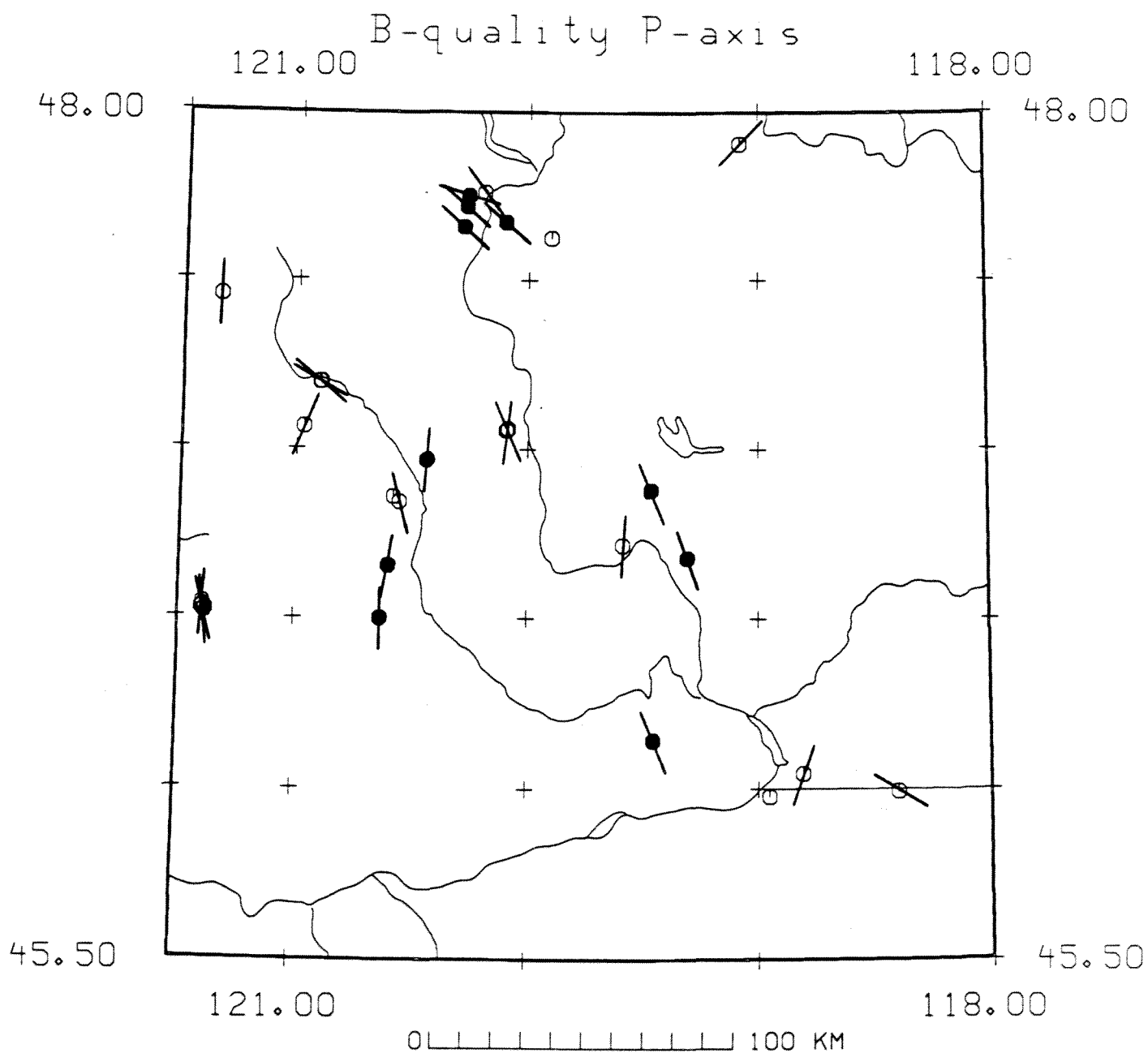


Figure III-7. Summary of orientation of P-axes for B-quality solutions. Events with a P-axis within 30° of horizontal have the horizontal projection of that axis shown as a line. Events whose T-axis is within 30° of vertical have filled symbols.

EARTHQUAKE SEQUENCE ANALYSIS

Introduction

Earthquakes have been classified as occurring in one of four types of sequences, based on their spatial and temporal location distributions and the temporal distribution of their magnitudes. These are foreshock-mainshock-aftershock sequences, mainshock-aftershock sequences, swarms, and single shocks. The cause for the different types of sequences has long been sought, and much work in fracture physics has been done on this behalf. One result of this work has been the suggestion that there is a relationship between the temporal pattern of seismicity and the degree of crustal heterogeneity or stress nonuniformity. A definitive answer to the cause of the different types of sequences is, however, far from being either proven or well understood. In addition, few detailed and comprehensive efforts have been made to determine what defines or at least typifies the temporal and spatial characteristics of the different types of sequences. A study aimed at characterizing the temporal and spatial patterns of the different types of sequences not only would improve our understanding of the earthquake generation process and rupture mechanics, but also has important implications for the discrimination of foreshock activity from swarm activity (i.e., earthquake prediction).

Eastern Washington is an ideal place to do such a study because all four types of sequences occur there and most of them occur within one geologic province, the Columbia Basin. This is a good situation because it is desirable to start with the simple case of comparing sequences that occur within one geologic province before we compare and attempt to understand sequences from varied geologic provinces. In studying only eastern Washington sequences, the differences in geology from one sequence to another are minimized and a comparison between different types of sequences will more likely yield understandable and meaningful results.

Previous Work with Eastern Washington Sequences

Various eastern Washington sequences have been studied. These include the Wooded Island swarms of 1969-70 and 1975, the Vantage swarm of 1974-75, the Wahluke swarm of 1972, the Eltopia swarm of 1973, the Royal mainshock-aftershock sequence of 1973-74, and the region of continuing high seismicity south of Lake Chelan. Because these studies used locations obtained from master event or standard location procedures, and because most of these earthquakes have small magnitudes ($M \leq 3.3$), errors in the relative locations of the earthquakes within a sequence are sure to exist. Intuitively, both the temporal and spatial distribution of earthquakes provide information on the changing state of stress in a region during an earthquake sequence. A sufficiently detailed analysis, in which precise relative locations of earthquakes are obtained, would provide valuable information about the earthquake generation process and the mechanics of rupture propagation. Performing this kind of detailed location analysis on the different types of sequences in eastern Washington will allow us to make comparisons between them, which may, in turn, yield basic differences or similarities among the four types of sequences.

Sequence Classification Procedure

Before we can perform a comparative analysis of different types of sequences, we must have an objective method of sequence classification. The first step in classifying a sequence is to identify, or define, the sequence. That is, we must determine which earthquakes are causally related to each other and hence form a sequence. The process of identifying a sequence is far from being simple. The spatial and temporal constraints necessary for the definition of a sequence are parameters that will vary with geographic location, magnitude, duration of the sequence, and, possibly, time. A sequence classification scheme must take into account this multivariate nature of the problem because we need to accurately and objectively identify sequences if we are going to compare the various types. Once a sequence has been identified, we can use the temporal

distribution of the magnitudes of the earthquakes within the sequence in order to classify the sequence as one of the four types. It is the development of such an objective sequence classification scheme that has been proposed as a Master's thesis and is currently in progress.

First Stage-- Procedure. The first stage of this Master's project has been completed. A computer algorithm has been written which, given a catalog of earthquakes, determines earthquake sequences. An earthquake sequence is defined as a set of earthquakes which fall within certain temporal and spatial bounds of each other and can therefore be assumed to be causally related. Specifically, given a temporal bound of T years and a spatial bound of X km, an earthquake is a member of a sequence if a) its epicenter lies no more than X km from the epicenter of at least one other earthquake in the sequence, and b) it occurs within T years of at least one other earthquake in the sequence. First we apply the spatial bound, or constraint, to an earthquake catalog to determine spatial clusters. Next, we apply the temporal bound, or constraint, to a spatial cluster to determine the sequences. Note that a sequence is a temporal clustering of earthquakes within a spatial cluster. Also note that if we let our temporal constraint be $T = \infty$ years, then a spatial cluster is itself a sequence.

At this point, a sequence has only been identified, not classified; that is, it can be any one of the four types of sequences (foreshock- mainshock-aftershock, mainshock-aftershock, swarm, or single shock).

First Stage-- Data and Results. Figures IV-1 through IV-4 demonstrate the algorithm, given four different pairs of spatial and temporal bounds. The earthquake catalog used in these figures is a subset of the University of Washington's catalog and consists of all earthquakes between 1 January 1980 and 30 March 1987 near Beverly, Washington, between latitudes 46.73°N and 46.85°N and longitudes 119.85°W and 120.10°W . There are no earthquakes outside this area that are within 5 km of any of the events shown.

The results presented in Figure IV-1 (read left to right, top to bottom) use a spatial constraint of 5 km and a temporal constraint of 150 days. Using these values, the earthquake catalog was divided into only one spatial cluster because all the earthquakes lie no more than the spatial bound of 5 km from another earthquake in the cluster. After applying the temporal constraint, the spatial cluster, labeled A on the far left of the figure, was subdivided into three sequences; these are depicted as the sets of "X's" within the three frames labeled A.1, A.2, and A.3. The labeling of the frames is as follows. The letter, in this case A, designates the spatial cluster. If there is a number following the letter and decimal point, it refers to a particular sequence within that spatial cluster. As mentioned above, the "X's" in each such frame (i.e., a frame whose label ends with a number) are the locations of earthquakes of that sequence. In addition, each of these frames shows, as octagons, the locations of earthquakes of all previously occurring sequences of the same spatial cluster. Looking successively at frames A.1, A.2, and A.3, then, one sees the progression of earthquake sequences with time. Frames that end with ".all" show the earthquakes of all the sequences of the spatial cluster whose designation is the letter which precedes the ".all". In accordance with this labeling procedure, the last frame in Figure IV-1, labeled A.all, shows all earthquakes in the spatial cluster A, regardless of time. Note that the largest distance between any two earthquakes in the spatial cluster is less than the spatial bound of 5 km.

Figure IV-2 shows the results when the spatial and temporal bounds were 5 km and 60 days, respectively. As in Figure IV-1, because the same spatial constraint was used, there is only one spatial cluster. Since the temporal constraint is smaller than the one used in Figure IV-1, more sequences could be expected, and indeed, 9 (rather than 3) sequences are defined within the spatial cluster. These are shown in frames A.1 through A.9. The last frame in Figure IV-2 (labeled A.all) shows all the earthquakes of that spatial cluster, regardless of time.

Figure IV-3 shows the results using spatial and temporal constraints of 3 km and

150 days, respectively. In this case, more spatial clusters are defined than in Figures IV-1 and IV-2. This could be expected since the spatial constraint is smaller than that used previously. The four spatial clusters are labeled A, B, C, and D at the far left of the figure. After applying the temporal constraint, each spatial cluster is subdivided into sequences; these are shown in the frames labeled A.1 and A.2, B.1, B.2, and B.3, C.1, and D.1. By comparing the frames labeled A.all, B.all, C.all, and D.all, each of which shows all the earthquakes of the corresponding spatial cluster, we can see that the distances between each of the spatial clusters is greater than the specified spatial constraint, i.e., 3 km.

Figure IV-4 is what we obtained using spatial and temporal constraints of 3 km and 60 days. The same spatial clusters are defined in this case as in Figure IV-3, because of the same spatial constraint, however the smaller temporal constraint results in more sequences within spatial clusters B and C.

Figures IV-1 through IV-4 demonstrate the fact that different spatial and temporal constraints define different sequences. That is, the set of "X's" in each frame of Figures IV-1 through IV-4 each define a sequence, and one can see, by comparing the figures, that the earthquake catalog can be divided into different sequences depending on the particular values chosen for the spatial and temporal bounds, or constraints. The algorithm accomplishes what has commonly been done subjectively in the description of an earthquake sequence. For example, for a foreshock-mainshock-aftershock sequence, one traditionally proceeds in the following way. First, the mainshock is identified. Then it is assumed that all earthquakes within a certain distance of the mainshock epicenter and within a certain time interval before and after the mainshock are causally related to the mainshock. Together with the mainshock, these earthquakes are then said to form a foreshock-mainshock-aftershock sequence.

Later Stages-- Proposed Work. The second stage of the proposed Master's project, currently in progress, is the development of a way in which the specified spatial and

temporal bounds used for defining sequences are treated as starting values and are systematically modified by the algorithm until optimum values are obtained. As mentioned earlier, the optimum values of the temporal and spatial bounds necessary to define a sequence vary not only from one geographic area to another (because of differences in background activity), but also vary from sequence to sequence (because of different maximum magnitudes and total durations of the sequences). To make things even more complicated, each of these factors may also be a function of time (for example, background activity in a particular area may increase or decrease with time). This is why it is difficult and perhaps overly simplistic to assign one pair of spatial and temporal constraints to a whole catalog of earthquakes if one expects to obtain reasonable results. This stage of the project, that is, determining the optimum spatial and temporal constraints needed to define any one sequence, involves developing quantitative ways to describe various statistical properties of sequences.

The third stage of the project is the actual classification of a sequence. One way to accomplish this may be to use the temporal distribution of the magnitudes within a sequence as the basis for classifying a sequence as one of the four types. For example, a foreshock-mainshock-aftershock sequence will have one significantly larger event (the mainshock) which occurs sometime after at least one smaller foreshock but is followed by the occurrence of smaller aftershocks. A swarm, in contrast, will have no event with a significantly larger magnitude than the rest.

Having thus identified and classified all sequences in a given catalog of earthquakes, the goals of the Master's thesis will have been achieved.

Concluding Remarks

Using an objective method of sequence classification such as the one briefly described above, a comparative study of sequences of each of the four types (foreshock-mainshock-aftershock, mainshock-aftershock, swarm, and single shocks) in Washington may be undertaken. Perhaps then we will be able to determine what properties typify

each of the different kinds of sequences and whether a particular area characteristically releases its seismic energy in the form of a certain type of sequence. This is a step towards determining what physical properties (geology, structure, etc) actually govern the occurrence of the different types of sequences.

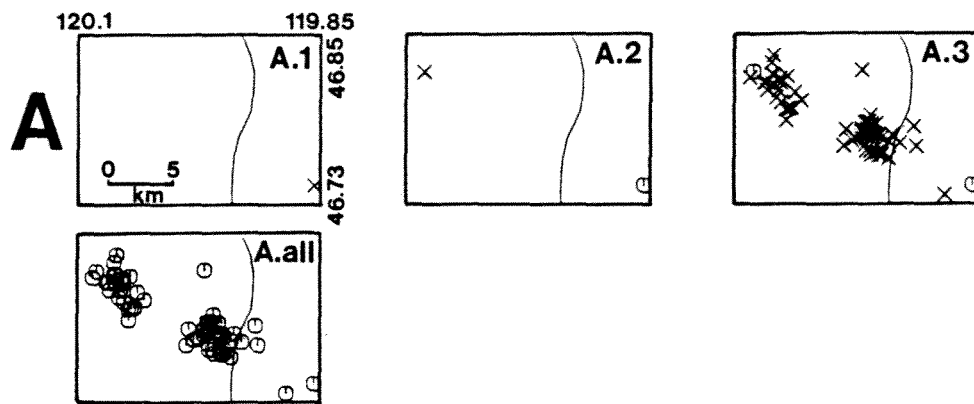


Figure IV-1. Earthquake sequences determined by using spatial and temporal constraints of 5 km and 150 days, respectively. See text for additional explanation.

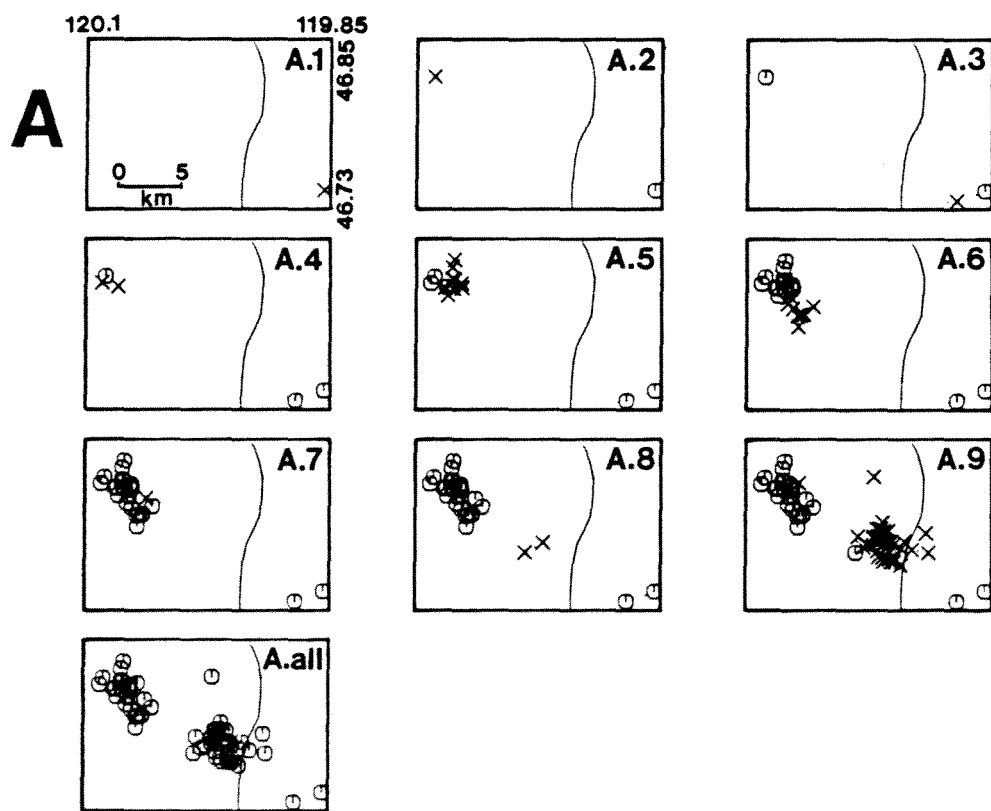


Figure IV-2. Earthquake sequences determined by using spatial and temporal constraints of 5 km and 60 days, respectively. See text for additional explanation.

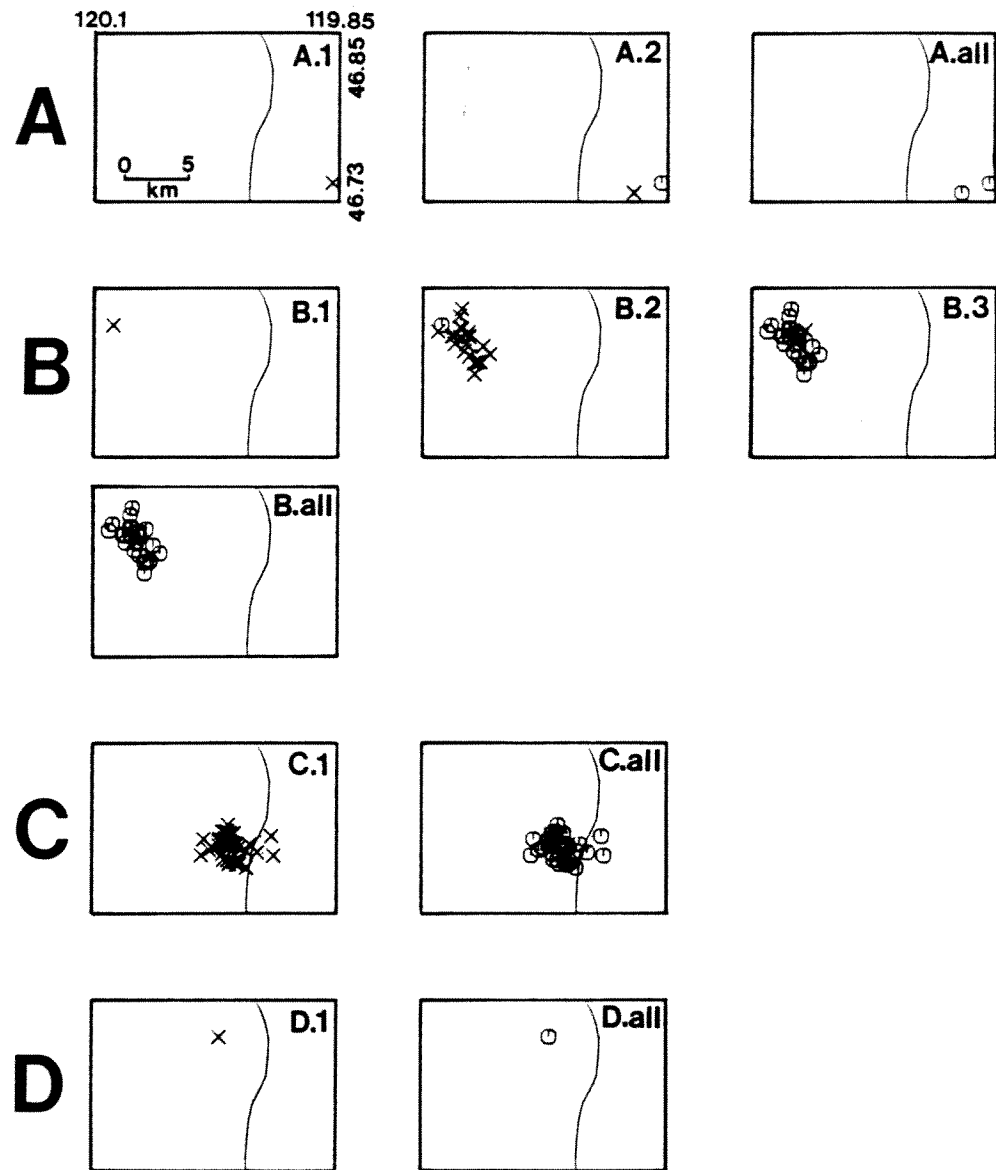


Figure IV-3. Earthquake sequences determined by using spatial and temporal constraints of 3 km and 150 days, respectively. See text for additional explanation.

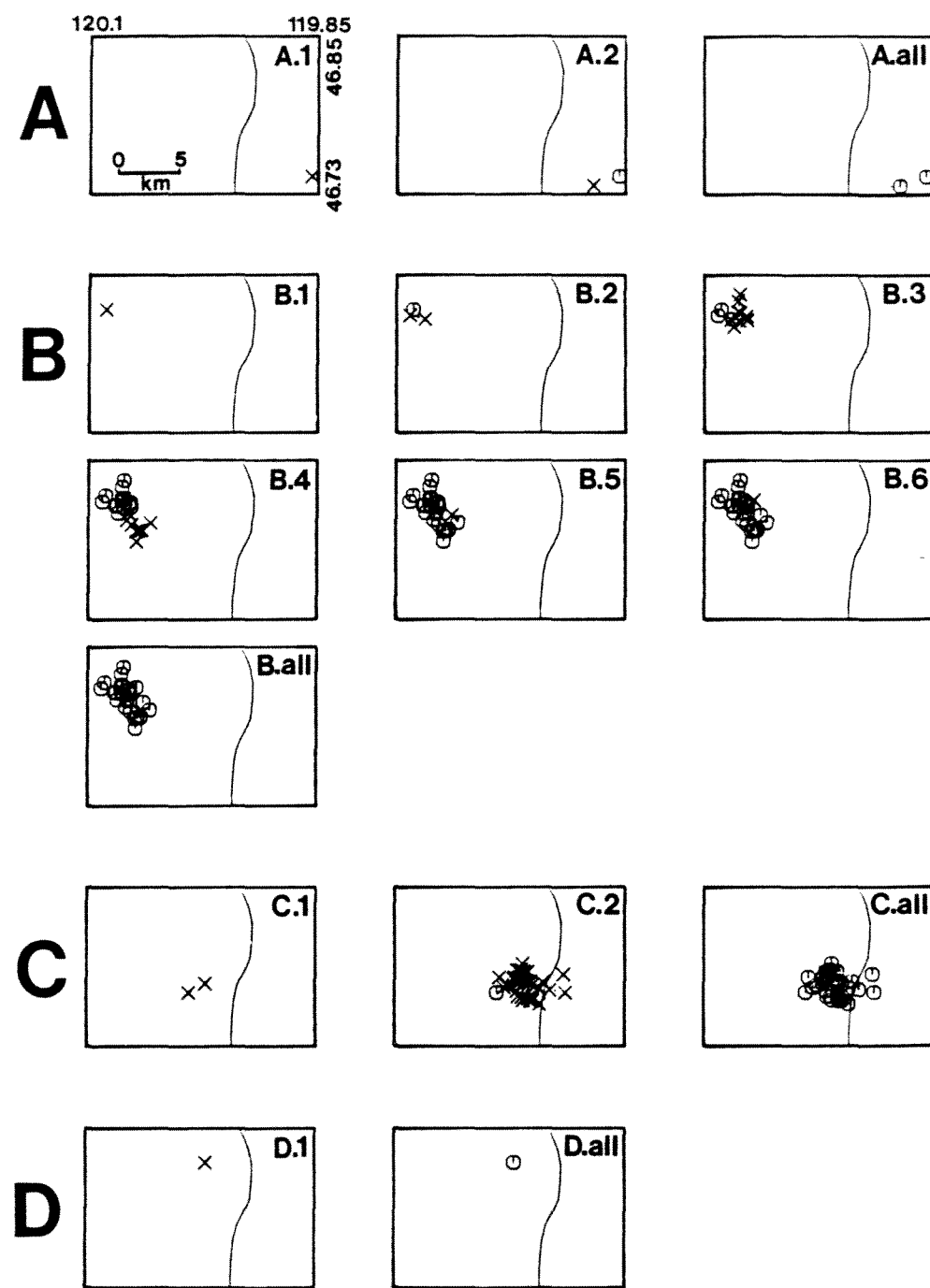


Figure IV-4. Earthquake sequences determined by using spatial and temporal constraints of 3 km and 60 days, respectively. See text for additional explanation.

HYPOCENTER DETERMINATION COMPARISON

Introduction

The computer location program called *spong* has been in use at the University of Washington for routine processing of data since 1981. It is a modified version of Bob Herrmann's program, *fasthypo*¹. While the original program has been used at several other institutions *spong* is primarily used here. It has never been checked in detail to see how its results compare with that of other similar programs.

The ability of a location program to accurately determine hypocenters is difficult to measure. Typically, synthetic data are used. Theoretical arrival times are generated for a hypothetical hypocenter and a given station set, and then the program is used to see how close its determined location comes to the original. One problem with this technique is the correct determination of travel-times between the known location and stations; ie generating accurate synthetic data. Without an independently verified travel-time calculator one can only use the travel-time calculator built into each location program. This suggests that the travel-time calculator should be checked separately from the hypocenter inversion portion of the code.

We have chosen three hypocenter determination programs to test, *spong*, our standard routine locating program, *lquake*, a location program by Bob Crosson² and *hypoinverse*, the well-known and popular program by Fred Klein³ used at the U.S. Geological Survey as well as other places. First we compared the travel-time calculators for each of these programs with each other. Since we have no way of knowing which of these travel-time calculators is correct (if any), this comparison is only useful to see what sort of differences may exist. Since there were slight differences between the three travel-time calculators we used each program's own routine to calculate synthetic arrival times in

¹Herrmann, R.B., FASTHYPO - a hypocenter location program. *Earthquake Notes* V50 #2 25-37, 1979

²Crosson, R.S., LQUAKE - location routine. University of Washington internal document, 1978

³Klein, F.W., *User's Guide to hypoinverse, a program for VAX and PC350 Computers to Solve for Earthquake Locations*. US Geological Survey Open File Report 84-000, 1984.

order to fairly test the location part of each program.

Travel-time Comparison

The travel-time calculator for each program was tested using two synthetic events, one shallow (1.3km) and one at a depth of 18.5km. The eastern Washington velocity model was used for these tests since it has several layers with rapidly changing velocities at shallow depths, and thus should be a worse-case type of model for accurate travel-time determinations. The two events were run through each program with hypocenters fixed. Since the arrival times at each station were made the same for the three programs the interesting output is in terms of residuals. The difference in the residuals from the three programs reflects differences in the travel-time calculators in each program.

The results are shown in figure V-1. The graphs are plots of distance from epicenter to station in kilometers versus difference in residuals between two programs in seconds. The closest comparison is between *spong* and *hypoinverse*. Over the distance range 0 to 150km (distance over which most travel-times are determined for routine network locations) the two programs compute travel-times within about 0.02 seconds of one another. At greater distances the differences increase to more than 0.2 seconds. This suggests that the travel-time calculator for these two routines generate similar results, at least for this model at distances important to our normal use. The travel-time calculator for the program, *lquake* seems to differ quite a bit from the other two programs. Even at close distances differences of as much as ± 0.2 seconds are observed and at distances of more than 150km, differences of almost 0.5 seconds are observed. At this point we do not know which of these routines calculates the true travel-time. We plan to investigate this apparent problem and resolve the discrepancy.

Location Determination

The second purpose of this study is to compare the results of the three earthquake location routines run under a series of realistic conditions. The ability of each program

to converge to a solution under varying conditions was tested to see if there were any problems or advantages to using one program over another.

Four events occurring in the past year, all located in Eastern Washington, were chosen as models from which to generate synthetic data for this study. Several criteria were considered in selecting these events including magnitude, location, and depth. The events all have magnitudes ranging from 2.0 to 3.0 so that readings from a large number of stations are available. Two events were located on the northern edge of the eastern Washington velocity model, one at a shallow depth and one at a deeper depth. Two other events are located in the center of the Pasco Basin, one shallow and one deep. The purpose of this configuration is to test a range of locations and array geometries.

The four events were run under a series of different conditions to see how the different programs would respond. To generate test data the hypocenter was fixed and the program run to determine travel-times to each station using the program's own travel-time calculator. These results were used to generate synthetic arrival-times at all stations. The program was then run with free parameters to see how close it could come to the original location under several different conditions.

First the unperturbed synthetic arrival times were just fed back into the programs. This should test each program's convergence criteria, and each program generated a location within its own convergence limit. Next, more realistic conditions were generated by reducing the number of stations in several stages and by the addition of noise to the arrival-time values. First only stations on one side of the event were used, then only the four closest stations, and then only the four farthest stations. Finally, noise was added to the synthetic arrivals of each event. Random values between +.5 and -.5 seconds were added to the arrival times. These particular tests were chosen because similar situations are encountered under realistic conditions, particularly for smaller events with weak arrivals, and it is important to know how each program handles these different cases. The distribution of stations relative to the synthetic epicenters is shown in figure

V-2 for the four situations used.

The results are presented in tables V-1 to V-4 organized by event. All values are given as the distance, in kilometers, from the relocated hypocenter to that of the fixed 'true' location. The first row contains the values the routines derived using all of the stations with perfect data. The next three rows contain values arrived at by reducing the number of stations in stages. The last two rows contain the values the routines calculated after adding random noise to the arrival times. The noisy events were run first using all of the stations, and then only eight evenly distributed stations. Places with no entry are cases in which the routine would not converge under that particular circumstance.

Table V-1 Shallow Source #1 (Z = 1.8km)

	SPONG		LQUAKE		HYPoinVERSE	
	Dist.	Depth	Dist.	Depth	Dist.	Depth
All Stations	0.01	0.00	0.00	-0.01	0.01	0.00
Southern half	0.02	0.00	0.02	0.00	0.04	-0.02
4 Closest	0.09	0.29	0.01	-0.08	0.04	-0.46
4 Farthest	0.04	0.02	0.01	0.01	---	---
Random noise	0.74	1.76	0.80	1.20	1.07	0.54
8 Sta +noise	1.08	1.75	0.45	0.06	0.85	1.75

Table V-2 Shallow Source #2 (Z = .4km)

	SPONG		LQUAKE		HYPoinVERSE	
	Dist.	Depth	Dist.	Depth	Dist.	Depth
All Stations	0.01	0.01	0.00	0.02	0.02	0.08
Eastern half	0.04	-0.08	0.15	-0.14	8.89	-8.01
4 Closest	0.00	-1.70	0.02	0.25	0.08	-2.74
4 Farthest	0.10	0.34	0.02	-0.01	78.91	-31.92
Random Noise	0.25	0.34	0.36	-0.01	0.34	-1.01
8 Sta +noise	2.64	-1.84	1.38	-0.65	31.97	-4.10

An examination of these tables shows that *lquake* does the best job of converging to the true hypocenter. In the worse case it was off only 2.58km in epicenter and 0.35km in depth. In most cases it was within 1.0km; even for rather difficult cases such as when using only the four farthest stations for a shallow event. The program *spong* does not

Table V-3 Deep Source #1 (Z = 17.2km)

	SPONG		LQUAKE		HYPOINVERSE	
	Dist.	Depth	Dist.	Depth	Dist.	Depth
All Stations	0.02	-0.01	0.01	-0.01	0.02	-0.02
Eastern	half	0.02	-0.01	0.03	-0.01	0.04
4 Closest	0.04	-0.01	0.12	-0.11	---	---
4 Farthest	0.02	3.77	0.00	0.00	---	---
Random noise	0.89	0.09	0.90	0.49	1.72	1.48
8 Sta +noise	0.19	0.49	1.20	1.07	4.54	8.73

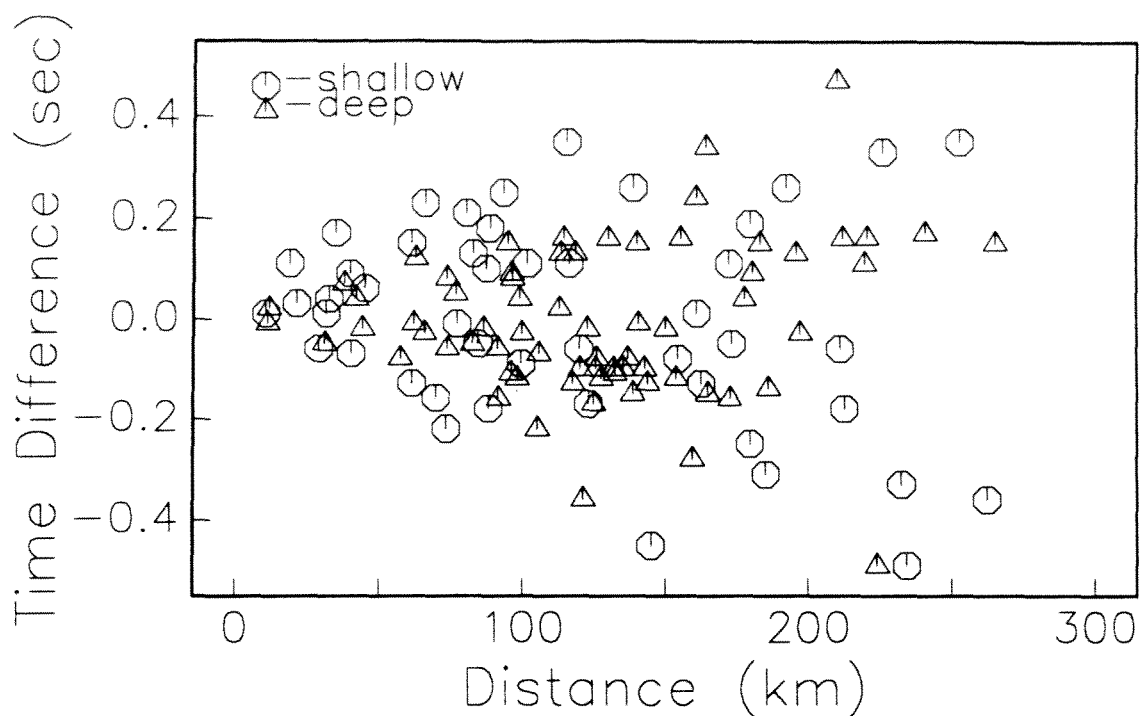
Table V-4 Deep Source #2 (Z = 19.5km)

	SPONG		LQUAKE		HYPOINVERSE	
	Dist.	Depth	Dist.	Depth	Dist.	Depth
All Stations	0.00	-0.01	0.03	-0.01	0.03	0.01
Southern Half	0.01	-0.05	0.02	0.01	---	---
4 Closest	0.03	-0.01	0.01	-0.03	0.02	0.02
4 Farthest	0.06	-0.84	0.05	0.00	54.25	-10.65
Random Noise	2.18	-0.35	2.32	-0.87	3.00	-2.11
8 Sta +noise	3.55	0.66	2.58	0.35	8.68	12.57

do much worse. Its largest error was 3.55km in epicenter and 3.77km in depth and it was no more than 1.0km off in most other cases. The program *hypoinverse* does very poorly in some cases. It failed to converge in a number of cases and was in error by as much as 78km in epicenter and 32km in depth in one case when it did converge.

This preliminary test of of these three location programs indicates that there may be problems with some of these programs which should be understood and corrected. The differences in the travel-time calculators is enough to make significant differences in locations from that source alone. Recall that the second test is independent of any errors in the travel-time calculator since each programs own routine was used to calculate the synthetic data for it. The inability of *hypoinverse* to adequately locate some of the test events indicates a potential problem with this very popular program. As a result of the above observations we are not satisfied that we understand the problems or limitations of these location routines and are continuing this investigation.

SPONG vers LQUAKE



SPONG vers HYPOINVERSE

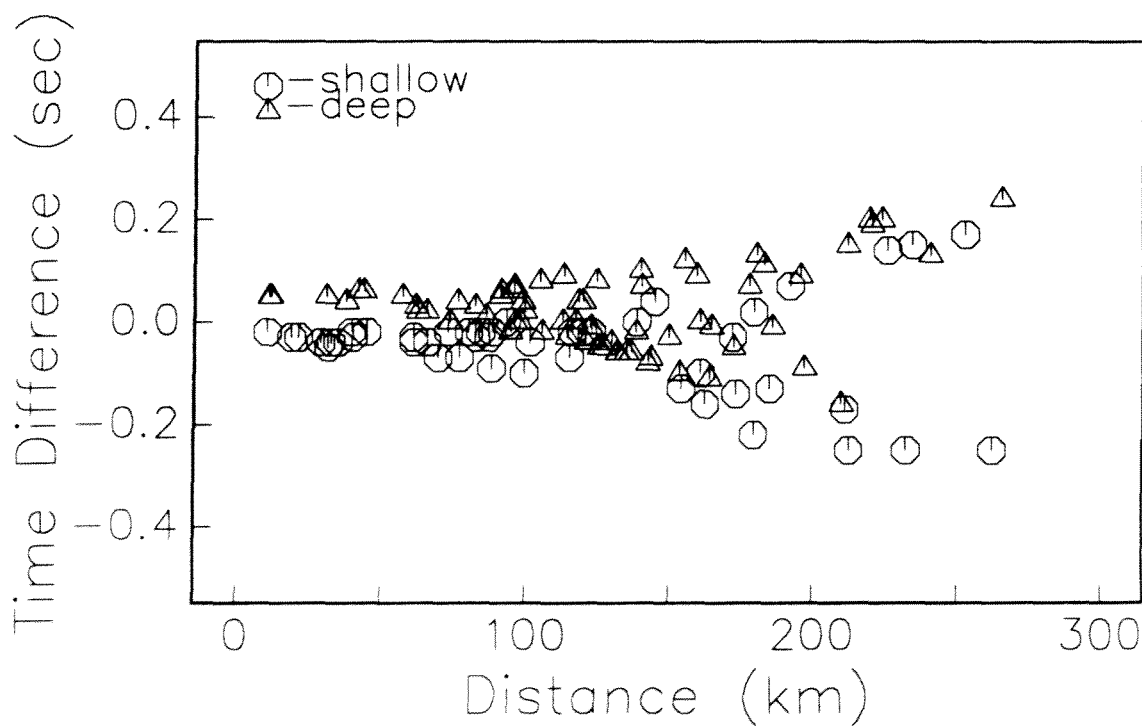


Figure V-1 Comparisons of travel-time calculators. The difference between calculated travel-times as a function of distance are plotted for a shallow source (1.3km) and a deep source (18.5km) for the programs *spong* minus *lquake* (top) and *spong* minus *hypoinverse* (bottom).

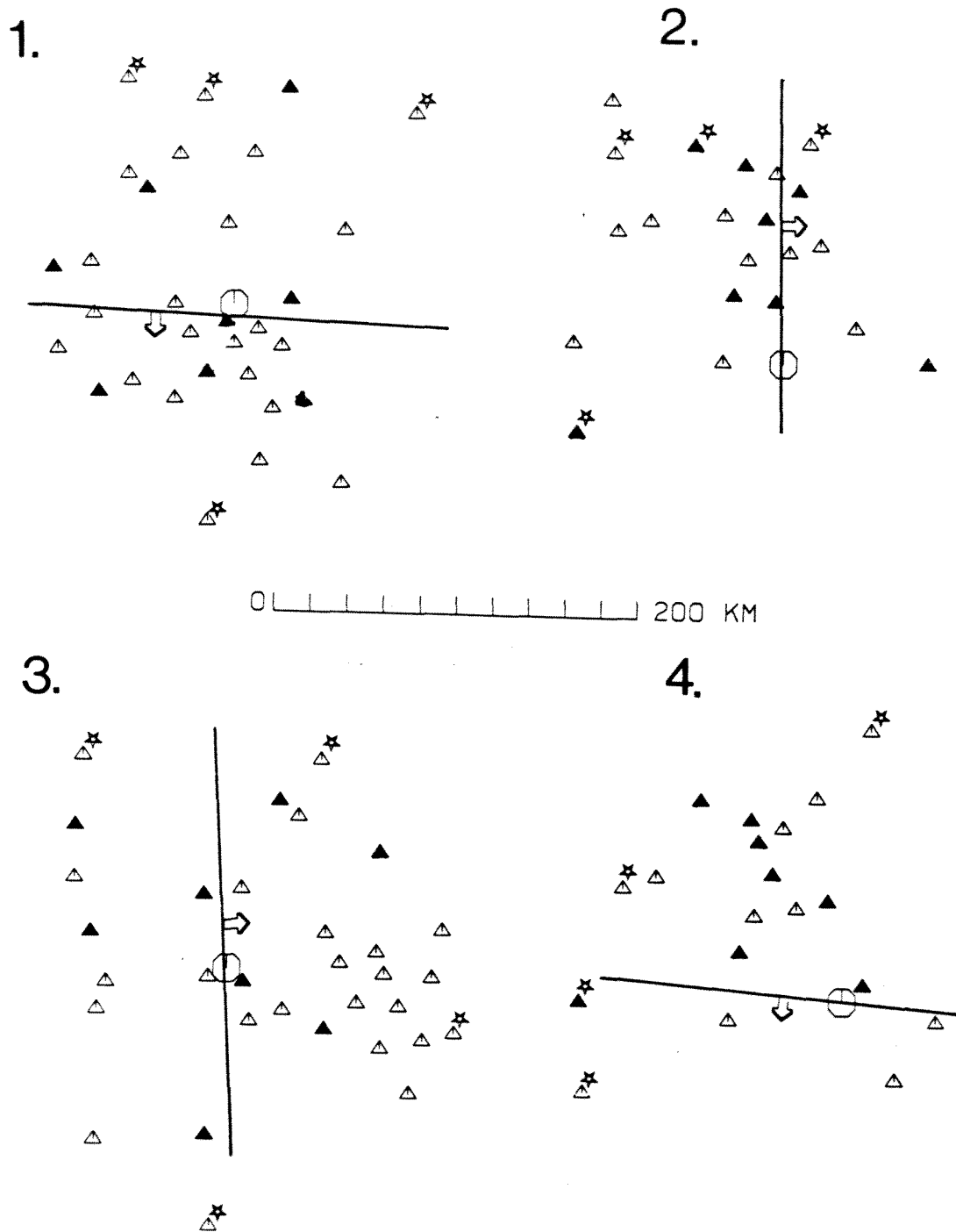
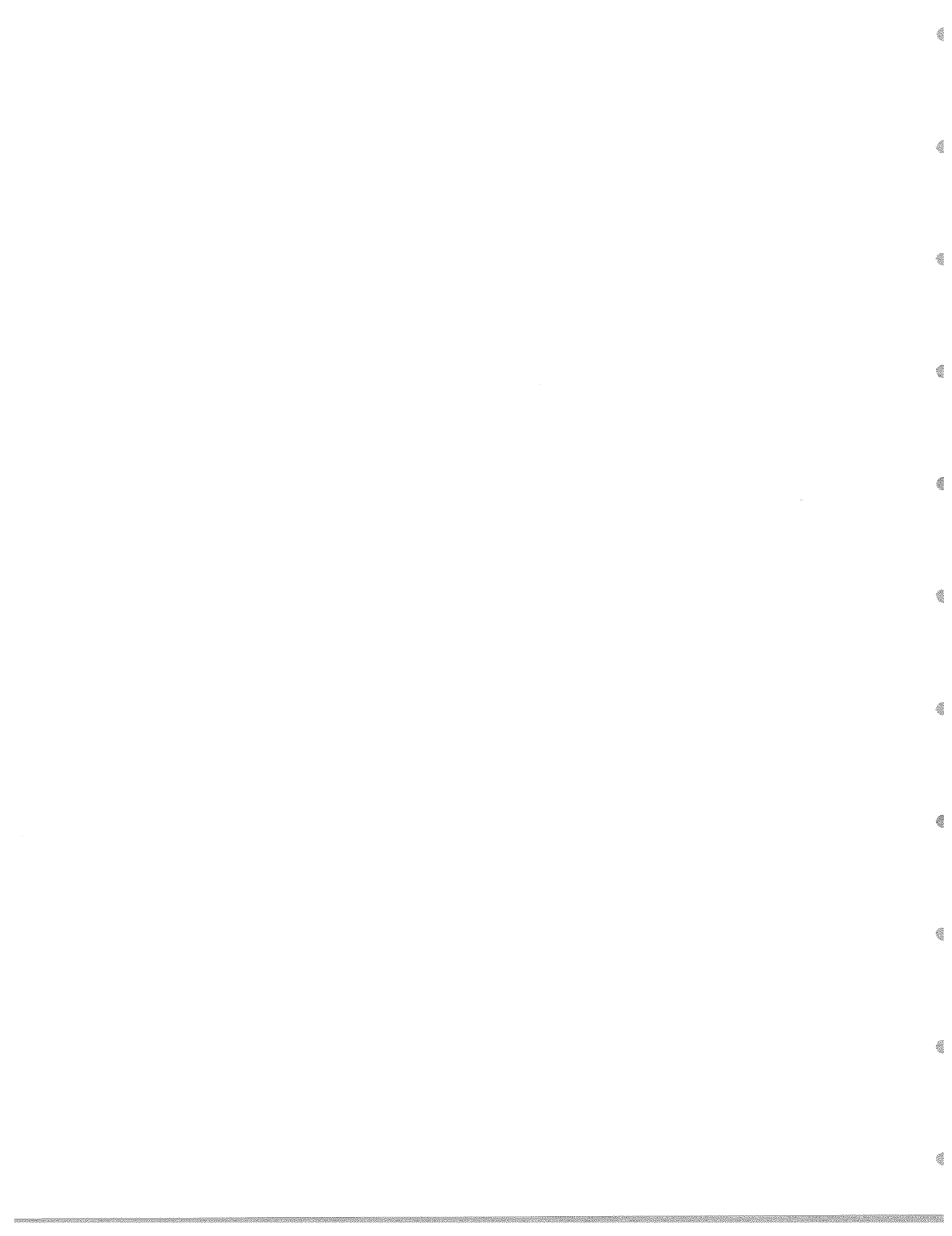


Figure V-2. Sketch maps showing the station-event geometry for the four cases summarized in tables V-1 to V-4. The circle is the earthquake epicenter. By rows from the tables the triangles are 'All Stations', the line with the arrow shows which 'half' of the stations are used, the '4 closest' stations have no special indicator, the '4 farthest' have stars by the triangle, and the '8 Stations' used with random noise have filled symbols.



CODA-Q Study

The following is an excerpt from a paper being prepared for submission to a seismology publication on a study of coda-Q in the state of Washington. This work was supported by several contracts including the current one and is of general interest to those studying the dependence of seismic wave attenuation on regional structure.

Introduction

Attenuation of seismic waves in the lithosphere at high frequencies (1-20 Hz) is an important property for the study of earth structure. One of the most useful parameters in describing this attenuation is the seismic quality factor Q , which contains meaningful information even at short distances.

Recently, Q determined from coda waves as well as from direct shear waves has been demonstrated to be a function of frequency, f , of the form

$$Q = Q_0 f^\alpha \quad (1)$$

where α is in the range 0.5 - 1.1. Both α and Q_0 show regional variation, often related to tectonic features. A strong correlation between the dependence of Q on frequency and the tectonic complexity of a region is sometimes observed. Areas of strong tectonic heterogeneity have strong frequency dependence of coda-Q as compared to that found in stable shield areas.

The state of Washington is a tectonically interesting area to study. There exist a variety of tectonic provinces, including active volcanos, and a subduction zone. Earthquake epicenters are widely distributed and depths range from near the surface to greater than 50km. The state is very well covered with short-period seismographs which are all digitally recorded on a computer system (figure VI-1). The intention of this study is to use data from the seismic network to calculate regional Q-values for the state of Washington and to try to relate these values to the local tectonics.

Data and Data Processing

In order to make a regional comparison of Q over the state, it is necessary to use the shortest possible station-event paths. This rules out simply selecting all the data with good signal-to-noise ratio since station-event distances would be quite variable and comparison between different areas difficult. The entire data base was searched to find the largest amount of useful data with the shortest possible hypocentral distances and the best signal-to-noise ratios. The thousands of events within a couple of kms of Mount St. Helens were excluded for the primary analysis.

After trying various combinations of selection criteria three different groups of data were obtained to give the best selection for the state-wide distribution of events and stations. Table VI-I lists the characteristics for these groups.

Table VI-1. Earthquake selection criteria for the different groups of events. The average t_p shows average P-travel times in each group of data actually selected.

Group name	Depth (km)	Max P-traveltime	Average t_p (sec)	Magnitude
Deep	> 35	12 sec	10	> 2.5
Medium	15 - 35	8 sec	6	> 2.5
Shallow	0 - 15	< 5 sec	4	2.5 - 3.0

Shallow events with magnitude larger than 3.0 were always clipped and for all of the groups the signal-to-noise ratio for most of the trace data was low for earthquakes with magnitude less than 2.5.

Traces of all event-station combinations in the University of Washington data files satisfying the above criteria were plotted as raw traces as well as band-passed filtered traces. Each plot was checked manually for data quality (duration, distortion, spikes, saturation and signal-to-noise ratio). More than half of the original data were rejected by visual inspection, mostly because of clipped signals or a low signal-to-noise ratio. The final data set consisted of 16 deep events (60 paths), 14 intermediate depth events (32 paths) and 65 shallow events (114 paths).

The original intention was to obtain enough data so that an individual Q -value could be calculated for each station using the average attenuation for at least 3-5 paths. However, with the above data set this was not possible and the data were, therefore, divided into groups covering different parts of the state. As a gross division between areas, boundaries between different major structural provinces were used. Divisions into smaller groups were done on the basis of the availability of data. The same division into areas was used for the 3 depth groups of data, although the deeper events provide Q information for western Washington only (figure VI-2). The division between areas is, of course, not very sharp and the volume of earth sampled for each area overlap quite a bit.

Individual event-station values for Q were determined as follows: The trace amplitude, $A(f, t)$ was obtained by bandpass filtering coda window trace data using a 6-pole Butterworth filter centered at frequency f , about one octave wide, and calculating RMS values using a sliding window of length $5/f$ seconds. Because of the relatively large lapse times and limitation in the bandwidth of our seismic network there was little energy left at frequencies above 16 Hz. Coda windows were selected automatically starting at twice the S-wave travel-time and were filtered at center frequencies of 2, 4, 8, 12, and 16Hz. Corresponding signal-to-noise ratios, maximum absolute trace values and Q were calculated for each frequency and plots were made showing each trace and the calculated values. An examples of such a plot is shown in figure VI-3.

Signal-to-noise ratios were automatically checked in all frequency bands by calculating the ratio between the RMS amplitude of the last 5 secs of the coda signal and the noise before the P-phase. Tests showed that signal-to-noise ratios less than 5 could affect the calculated Q values, thus such data were rejected as unusable. For each trace a value of Q was calculated. Results with regression correlation coefficients less than 0.45 were not used. The value of 0.45 is somewhat arbitrary, but represents a compromise between rejecting too much data and obtaining a high scatter in individual Q values for

a particular area.

Initial results from the groups of shallow events, using the criteria $t_{start} = 2t_S$ showed apparent regional differences in Q . However, it turned out that these small differences were systematically proportional to differences in average lapse times, t_{start} , for the different groups. Because of nonuniformity of earthquake distribution, some regions were favored by significantly smaller average lapse times than others resulting in apparent differences in Q values. These differences disappeared when the same t_{start} were used for all groups. The start time of the coda window was then chosen to be 18 sec after the origin time, which corresponds to $2t_S$ assuming a max P-travel-time of 5 secs.

Similar tests were also made on the data for the intermediate and deep events. Using a constant t_{start} for all events increases the t_{start} to 29 and 43 secs for the intermediate and deep groups respectively; and thus, on average increasing t_{start} by 6 and 7 secs respectively. These long lapse times, unfortunately, reduced the amount of data by almost half since the signal-to-noise ratio is reduced considerably for these longer lapse times. The results using constant t_{start} and the criteria $t_{start} = 2t_S$ gave almost the same results. This can be explained by the fact that the lapse time is already large and therefore small changes in lapse time should affect the results much less than for the shallow events where lapse times were much smaller. The final processing was done with a fixed $t_{start} = 18$ sec for the shallow events and $t_{start} = 2t_S$ for the other two groups.

In order to make a meaningful comparison of Q from different regions it is important to make estimates of the volumes sampled by the different groups of data. Assuming that the maximum volume sampled by the coda waves at time t is an ellipsoid with semi-major axis $a_1 = v_S t / 2$ and semi-minor axis $\sqrt{a_1^2 - \Delta^2 / 4}$, where Δ is the source-station distance (Pulli, 1984), approximate volume estimates can be made. The maximum t will be $t_{start} +$ window length; however, the average volume sampled can be assumed to be $t_\Delta = t_{start} + L_{window} / 2$. Table VI-2 shows the calculation of a_1 and a_2 for the

different groups of data. Δ has been calculated from the average P-travel time (Table VI-1) assuming an average P-velocity of 7 km/sec. As the table shows, a_1 and a_2 are very similar, so the sampled volume is nearly a sphere. Using the average depth in each depth group, h_{av} , a reasonable estimate of the maximum depth of the volume is then $a_2 + h_{av}$ as indicated in Table VI-2.

Table VI-2. Estimate of volumes sampled by the coda waves in the different groups. Average depth- h_{av} , window start time- t_{start} , average hypocentral distance- Δ , semi-major and semi-minor axis- a_1 and a_2 , and maximum depth of that volume.

Group	Shallow	Medium	Deep
h_{av} km	6	21	47
t_{start} sec	18	19	22
Δ km	28	42	70
a_1 km	55	57	63
a_2 km	53	52	52
max depth	59	73	99

The areal extent of a region depends on the coverage of the stations and events in a particular group and extends out about a_1 km. The calculated maximum depth, a_1 , and a_2 must be considered approximate and subject to local conditions since some strong assumptions have been made, namely constant velocity and constant density of scatterers.

For each area, average Q-values and standard errors were calculated at each frequency and a fit to equation (1) was made, calculating α and Q_0 . In order to facilitate a comparison between different areas, a fit to equation 1 was also made with α fixed to its average value (usually 1.0, see below) and only Q_0 was calculated. Finally an average of the whole state was obtained for data in each depth group by averaging the values for each group.

RESULTS

All results using the standard 20 sec coda window are given in Table VI-3. In order to facilitate the comparison between regions, plots of Q vs f are shown in two different combinations in figure VI-4 and VI-5. Figure VI-4 shows a comparison between Q in the

different regions for each depth group and figure VI-5 shows a comparison between Q for the four depth groups for regions *East*, *West*, *North* and *Puget* (see figure VI-2 for location of regions). $Q(f)$ for the different groups turned out to be quite similar and standard errors for some combinations rather large (Table VI-3). In many cases, one $Q(f)$ curve is not distinguishably different from another within \pm one standard errors. It is obvious that for all data groups, that Q increases almost linearly with frequency with $\alpha = 0.9-1.1$. Most of the individual sub-groups can not be easily distinguished from each other when taking into account the calculated errors (Table VI-3).

Results from the shallow group are shown on figure VI-4c. Although the scatter in the data is large, there are minor indications of regional differences. At lower frequencies (2, 4, and 8 Hz) the Puget Sound area (*Puget*) seems to have consistently higher coda-Q values than the rest of the areas. There is especially a contrast with the *west* and *North* areas at a frequency of 8 Hz which also can be seen in the data using the medium depth group of events (figure VI-4b). The differences in Q between areas *North* and *Puget* are greater than their standard errors and therefore seem to be real and probably due to crustal differences in coda-Q. Another clear difference between area *North* and all the other regions is that α is consistently low (0.7-0.8) for all depth groups while the other groups of data do not show any consistent α variation from the average α of 1.0 (figure VI-5). Since this is seen in all depth groups, especially the deep events, this difference in α may also exist below the crust, and could be an effect of only subcrustal structure since all three depth groups sample below the Moho (Table VI-2).

A comparison of Q grouped by areas (figure VI-5) shows that for area *North*, there is almost no change in Q with depth, for areas *West* and *East* deeper events show slightly higher Q , while for area *Puget*, shallow events give higher Q than the deeper events. In most other studies Q has been shown to increase with depth. This only seems to be marginally the case for areas *East* and *West* in Washington.

The state-wide averages of $Q(f)$ (Table VI-3) are quite similar for the three depth

groups although lapse times are quite different (Table VI-2). This seems to indicate, that in general, Q does not change much with depth.

The method used here is not very sensitive to possible Q -variations in the very shallow part of the crust since the minimum t_{start} which can be used is 18 seconds implying an sample volume with a radius of about 50km. At least below the crust there seems to be little variation in Q with depth. This observation is quite different from most other coda Q studies which, in general, report increases in Q with longer lapse times, including lapse times longer than used in this study (e.g. Pulli, 1984, Rautian and Khal-turin, 1978).

DISCUSSION

The small regional variation in Q might seem surprising considering the large variation in the tectonics and crustal structure (Crosson, 1974; Geophysics Program, 1977, 1985). Larger variations might have been seen if smaller lapse times could have been used and therefore Q for very shallow structures determined. The similarity of the state-wide Q values seem to indicate that the average attenuation properties and distribution of scatters in the whole crust and part of the upper mantle are similar. A study of regional differences in the coda duration versus local magnitude relation, published in our annual technical report, 1977, found that the same relation could be used in eastern Washington as that used in western Washington. Since the end of the coda wave train used for coda duration magnitude calculations is made up of predominantly energy around 1-5 Hz, this observation independently supports the present study indicating similar values of coda- Q throughout the State.

This result appears to be inconsistent with another study comparing the attenuation patterns from large earthquakes in Washington State (Malone and Bor, 1979). In this study the isoseismal distribution for earthquakes east of the Cascades were spread over a larger area for an earthquake of a given magnitude than for a similar earthquake west of the Cascades. This would imply that the attenuation of strong seismic waves is

lower in the east than in the west which is inconsistent with the current coda-Q study. It is possible that the strong shaking used for intensity studies is not due to back-scattered coda waves and thus two different types of attenuation are being measured by these two studies.

The lack of an obvious depth dependence of Q in parts of Washington is in contrast to most other areas for which similar Q investigations have been done. It seems that the average Q does not change much over the top 100km of the crust and upper mantle, at least in the Puget sound area, while there is only a slight increase of Q with depth in eastern Washington. This may partially be due to the limited frequency band and comparatively short lapse times used in the current study.

TABLE VI-3

CODA-Q OF THE STATE OF WASHINGTON											
Group Name	f	2.0	4.0	8.0	12.0	16.0					
	Δf	0.75	1.5	3.0	4.0	6.0					
<i>North</i>	<i>Q</i> -shallow	116	285	444	583	745	Q_0	σ_d	α	σ_d	ρ
	σ	9	49	27	42	37	81	5	0.81	0.03	0.99
	N	2	4	7	6	7	N_T	H	t	C_Q	σ_d
							26	6	18.0	54	8
	<i>Q</i> -medium	157	260	436	638	690	Q_0	σ_d	α	σ_d	ρ
	σ	5	26	47	40	45	93	3	0.75	0.01	1.00
	N	3	5	5	4	2	N_T	H	t	C_Q	σ_d
							19	20	22.3	59	10
	<i>Q</i> -deep	157	230	413			Q_0	σ_d	α	σ_d	ρ
<i>N. West</i>	σ	13	36	47			86	6	0.75	0.04	0.99
	N	2	4	2			N_T	H	t	C_Q	σ_d
							8	51	34.5	59	11
	<i>Q</i> -deep	90	204	546			Q_0	σ_d	α	σ_d	ρ
	σ	14	27	77			37	1	1.28	0.02	1.00
<i>West</i>	N	7	5	3			N_T	H	t	C_Q	σ_d
							15	42	36.2	51	9
	<i>Q</i> -shallow	136	188	356	688	1682	Q_0	σ_d	α	σ_d	ρ
	σ	11	10	41	107	199	59	6	0.97	0.06	0.94
	N	11	12	5	3	2	N_T	H	t	C_Q	σ_d
							33	3	18.0	51	16
	<i>Q</i> -deep	127	269	498	688	1085	Q_0	σ_d	α	σ_d	ρ
	σ	9	21	31	55	123	65	1	0.99	0.01	1.00
	N	27	21	13	9	8	N_T	H	t	C_Q	σ_d
<i>South</i>							78	47	32.7	64	3
	<i>Q</i> -medium	90	231	437	868		Q_0	σ_d	α	σ_d	ρ
	σ	28	66	36	67		41	4	1.18	0.05	0.99
	N	2	2	2	2		N_T	H	t	C_Q	σ_d
							8	23	22.7	57	10

 σ = Standard error of the mean σ_d = Standard deviation

CODA-Q OF THE STATE OF WASHINGTON (cont.)											
Group	f	2.0	4.0	8.0	12.0	16.0					
<i>Central</i>	<i>Q</i> -shallow	124	199	471	676	917	<i>Q</i> ₀	σ_d	α	σ_d	ρ
	σ	17	21	34	82	97	59	2	0.98	0.02	1.00
	N	9	7	8	7	5	<i>N_T</i>	H	<i>t</i>	<i>C_Q</i>	σ_d
<i>Puget</i>	<i>Q</i> -shallow	154	318	650	742	839	<i>Q</i> ₀	σ_d	α	σ_d	ρ
	σ	31	26	39	61	72	100	6	0.80	0.03	0.98
	N	4	4	5	10	9	<i>N_T</i>	H	<i>t</i>	<i>C_Q</i>	σ_d
<i>East</i>	<i>Q</i> -medium	128	283	509	726	882	<i>Q</i> ₀	σ_d	α	σ_d	ρ
	σ	23	31	31	42	59	73	2	0.92	0.01	1.00
	N	7	9	14	12	9	<i>N_T</i>	H	<i>t</i>	<i>C_Q</i>	σ_d
<i>Group Average</i>	<i>Q</i> -deep	121	235	485	688	783	<i>Q</i> ₀	σ_d	α	σ_d	ρ
	σ	19	28	47	79	45	63	1	0.96	0.01	1.00
	N	9	7	8	5	2	<i>N_T</i>	H	<i>t</i>	<i>C_Q</i>	σ_d
							31	48	33.3	59	3
<i>East</i>	<i>Q</i> -shallow	96	226	513	827	940	<i>Q</i> ₀	σ_d	α	σ_d	ρ
	σ	9	30	92	82	56	45	1	1.14	0.01	1.00
	N	13	8	4	8	7	<i>N_T</i>	H	<i>t</i>	<i>C_Q</i>	σ_d
<i>Group Average</i>	<i>Q</i> -medium	143	292		1280		<i>Q</i> ₀	σ_d	α	σ_d	ρ
	σ	18	14		153		69	8	1.02	0.06	0.99
	N	2	3		2		<i>N_T</i>	H	<i>t</i>	<i>C_Q</i>	σ_d
							7	19	18.1	71	8
<i>Group Average</i>	<i>Q</i> -shallow	129	228	479	711	955	<i>C_Q</i>	<i>Q₀</i>	α	ρ	
	σ	27	45	89	97	213	60	63	0.97	1.00	
	<i>Q</i> -medium	124	264	448	755	912	<i>C_Q</i>	<i>Q₀</i>	α	ρ	
	σ	32	29	37	108	230	61	66	0.96	1.00	
	<i>Q</i> -deep	119	232	481	657	910	<i>C_Q</i>	<i>Q₀</i>	α	ρ	
	σ	28	26	57	52	208	58	61	0.98	1.00	

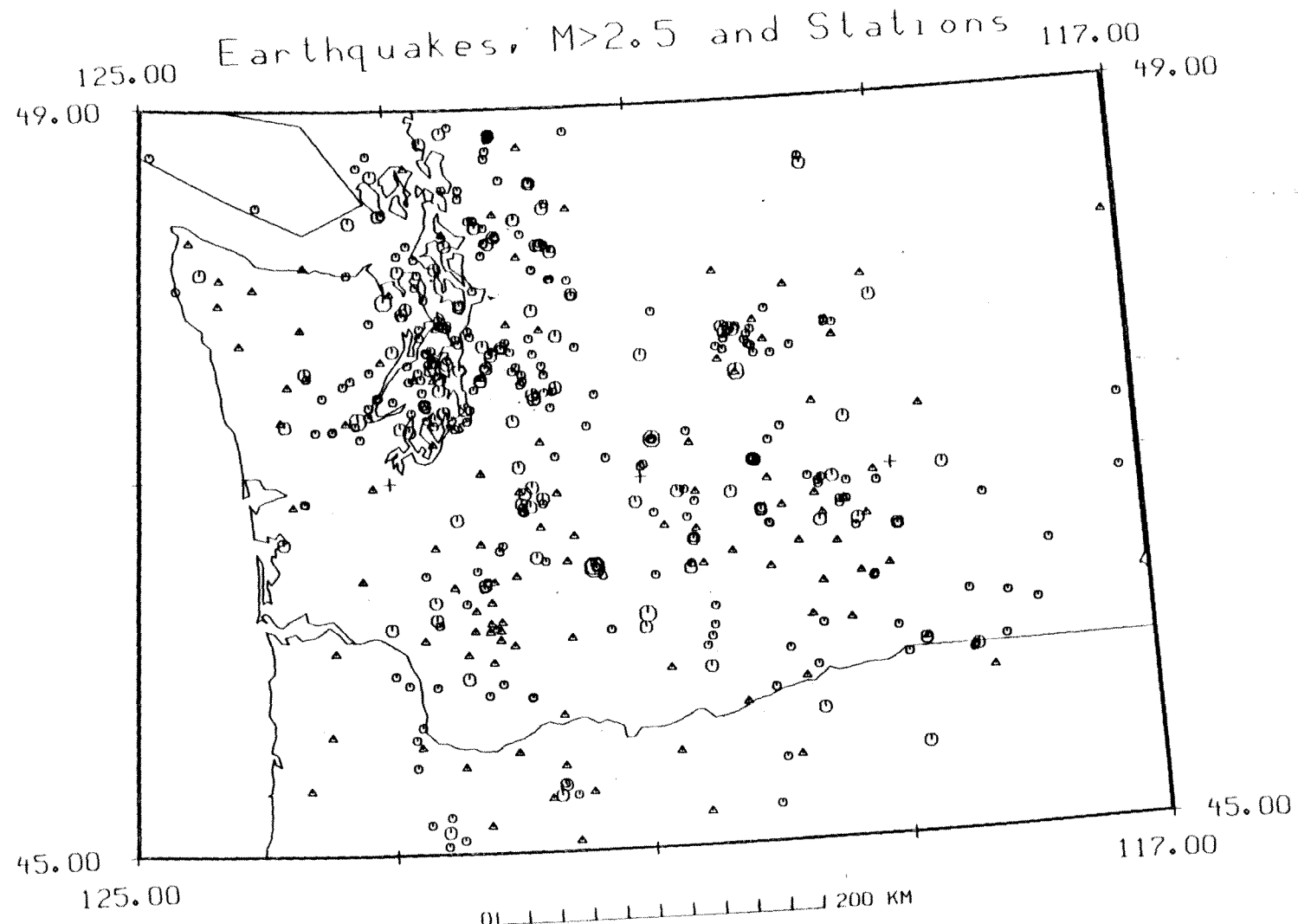


Figure VI-1. Map showing the seismograph stations of the University of Washington state-wide network as triangles and the earthquakes selected for this study as circles. The heavy lines divide the region into provinces for which different velocity models have been determined.

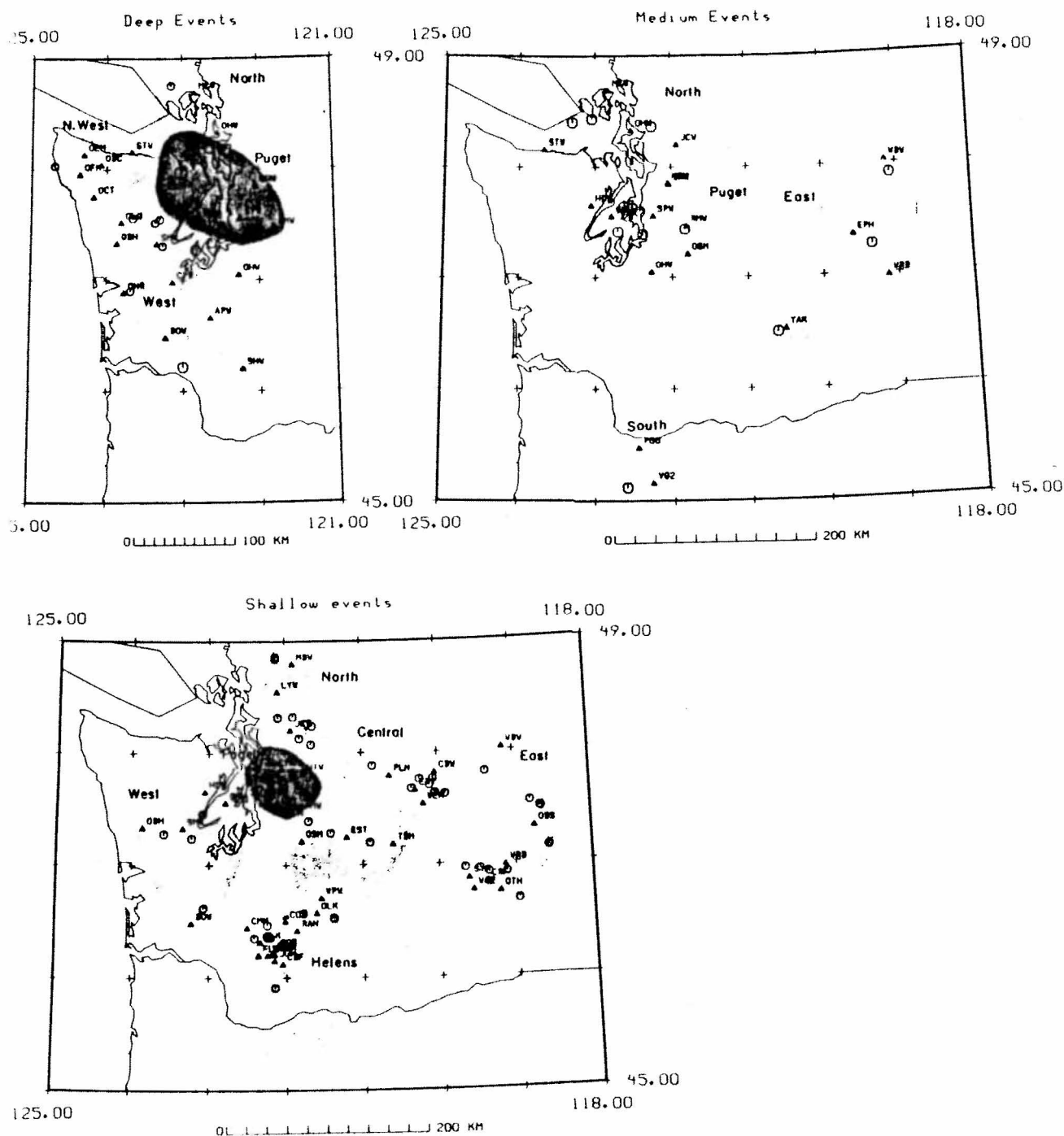


Figure VI-2. Maps showing the event-station combinations grouped by depth. Triangles are stations with their names; circles are the earthquake epicenters; the shaded areas are the rough outlines of the sampled areas for each sub-group.

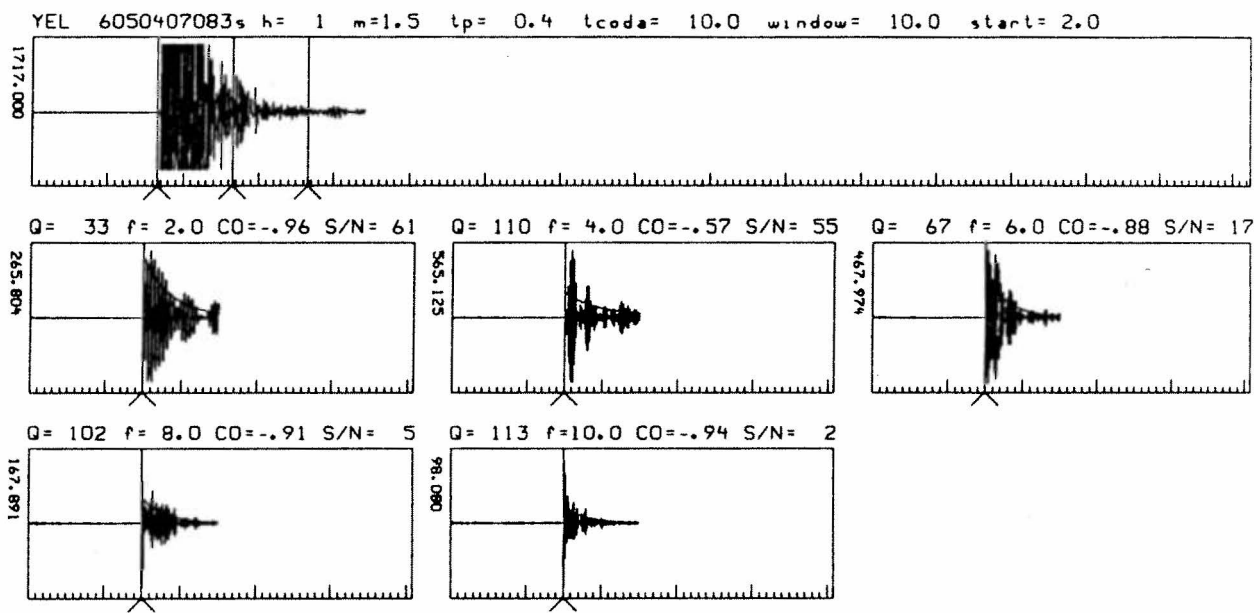


Figure VI-3. Examples of an unfiltered and bandpass filtered traces for a medium deep event from central Puget Sound. The top trace is the original unfiltered data trace where the 3 vertical lines indicate (from left) origin time, start and end of coda window. Above the first trace is first given the station code and event identification. The abbreviations are: h: depth (km), m: magnitude, tcoda: start of coda window measured from the origin (sec), window: window length (sec), start: start of coda window expressed as a multiple of S-travel times (tcoda is always > start * S-travel time), f: frequency (Hz), Co: correlation coefficient, and S/N: signal to noise ratio of last 5 secs The fit to each filtered segment is shown as a decaying curve.

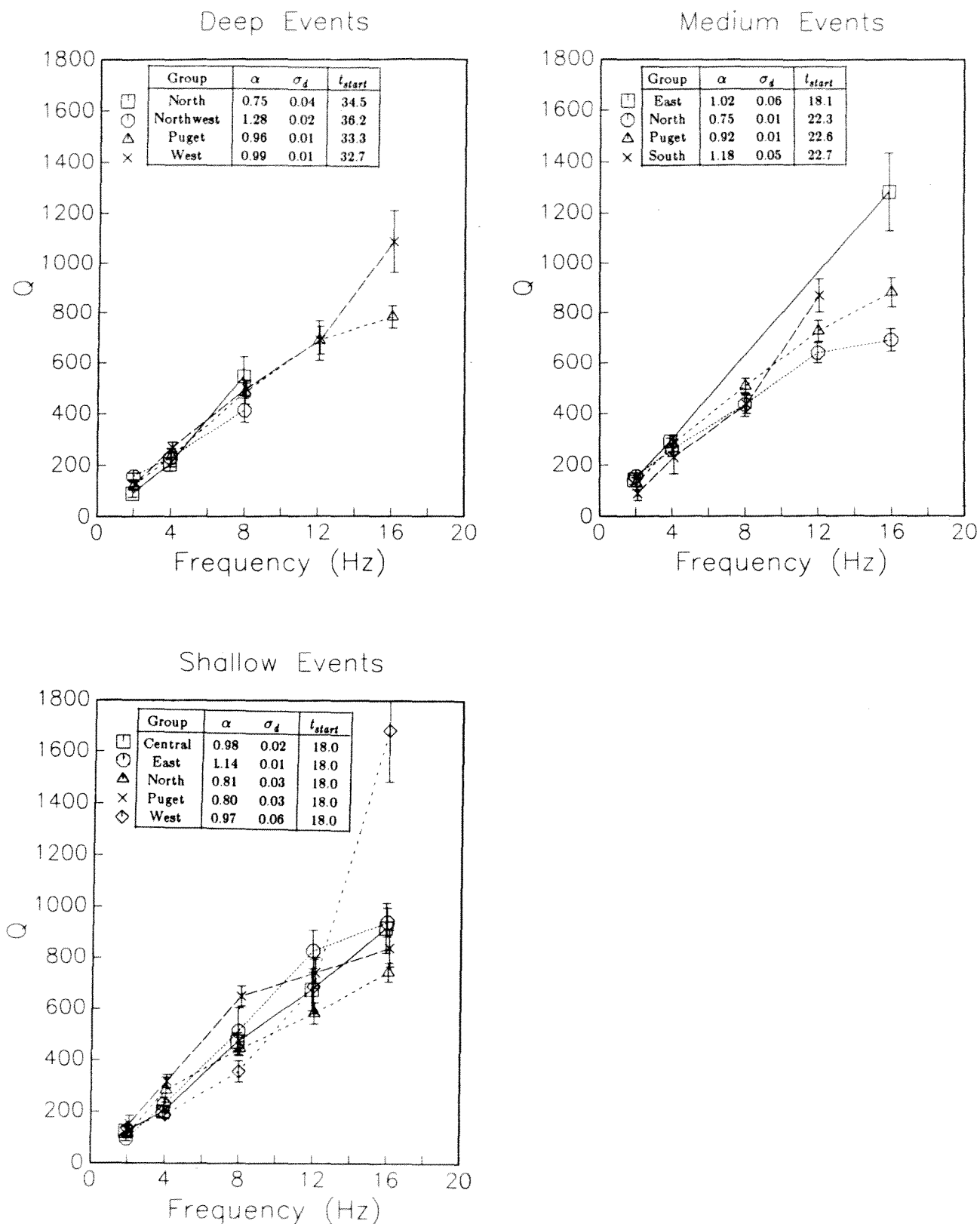


Figure VI-4. Q versus frequency plotted by depth group. In the table α is the average slope of the best fit frequency dependence and t_{start} is the window start time in sec.